Temporally overlapping mechanisms diversify clonal B cell responses *in vivo.*

Oliver P. Skinner[1]*, Saba Asad[1]*, Marcela L. Moreira[1], Hyun Jae Lee[1], Cameron G. Williams[1], Shihan Li[1], Wang Jin[2], Thiago M. Steiner[1], Takahiro Asatsuma[1], Jorene Lim[1], Zheng Ruan[1], Megan S.F. Soon[3], Jessica A. Engel[4], David S. Khoury[2], Zewen Kelvin Tuong[3], Hamish W. King[5,6], Ashraful Haque[1¶]

*These authors contributed equally

Affiliations

[1]Peter Doherty Institute for Infection and Immunity, Department of Microbiology and Immunology, University of Melbourne, Parkville, Victoria, Australia
[2]Kirby Institute, University of New South Wales, Kensington, New South Wales, Australia
[3]Ian Frazer Centre for Children's Immunotherapy, Child Health Research Centre, Faculty of Medicine, University of Queensland, Australia
[4]QIMR Berghofer Medical Research Institute, Herston, Brisbane, Queensland, Australia
[5]The Department of Medical Biology, The University of Melbourne, Parkville, Victoria, Australia
[6]Epigenetics and Developmental Division, Walter and Eliza Hall Institute of Medical Research, Parkville, Victoria, Australia

*Authors contributed equally
[¶]Corresponding author: Associate Professor Ashraful Haque, 792 Elizabeth Street, Melbourne, VIC 3000, Australia, e-mail: ashraful.haque@unimelb.edu.au, tel: +613903355206

Abstract

Single naive B cells amplify and diversify their responses when activated by cognate antigen, via *Myc*-dependent clonal expansion, immunoglobulin class switch recombination (CSR), phenotypic variation, and somatic hypermutation (SHM). Whether these mechanisms act combinatorially *in vivo* to diversify clonal responses to a single complex pathogen remains unclear. Since diversity in the antigenic targets, functional classes, and production kinetics of parasite-specific antibodies influences immunity to malaria, we test here whether individual B cell clones diversify over time during *Plasmodium* infection and treatment. During the first week of infection, amid widespread Type I Interferon (IFN)-mediated, bystander activation, CSR initiates soon after *Myc* up-regulation. CSR then overlaps with clonal expansion, resulting in isotype variegation amongst certain clones. In the second week of infection, expanded clones seeding germinal centres (GC) both bifurcate into extra-follicular plasmablasts and exhibit isotype variegation, revealing substantial intra-clonal diversification. Over the following month, GC clones undergo SHM at approximately four mutations per week, with IgG mutational diversity and IgM$^+$ cells preserved in GCs over time. Anti-malarial intervention does not impede SHM, but instead exerts quantitative limits on GC size, plasma cell emergence and circulating antibody titres. Finally, we reveal a contemporaneous B cell developmental pathway that relocates from bone marrow to the spleen during infection and treatment. Thus, multiple temporally overlapping mechanisms combine *in vivo* to amplify, diversify, and safeguard humoral immune responses.

Graphical abstract

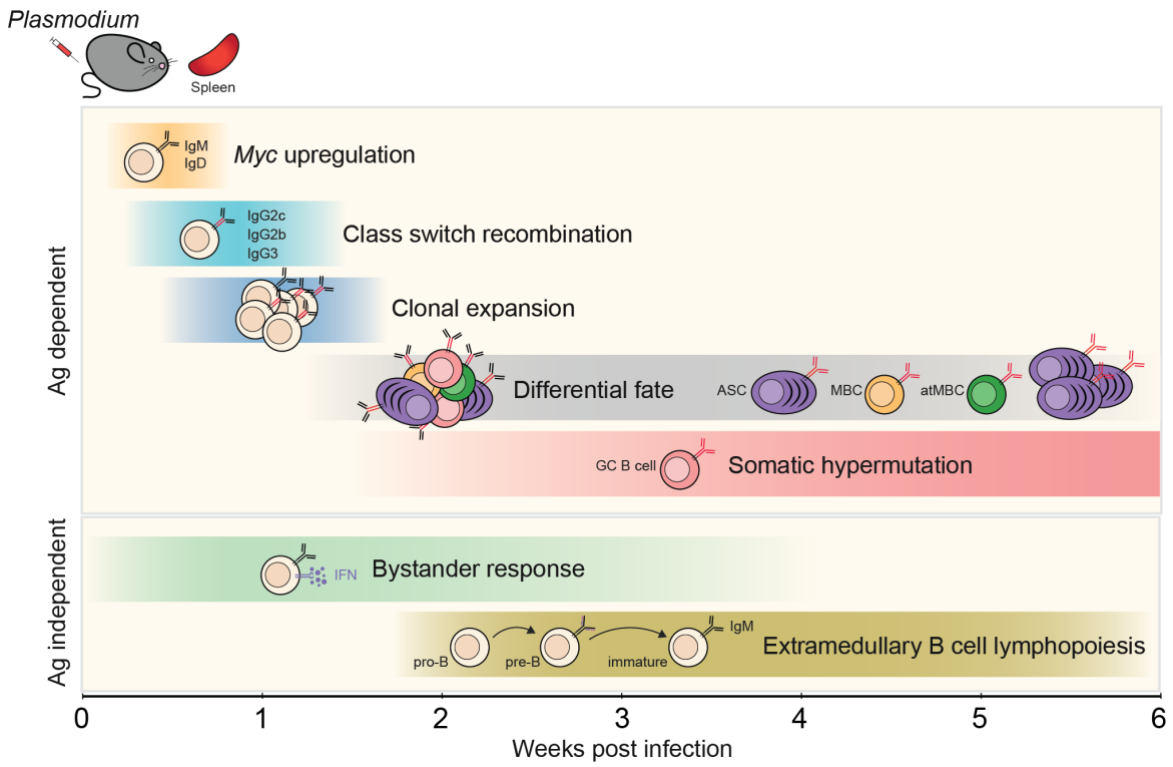

Highlights:

- Early temporal overlap of CSR with clonal expansion leads to isotype variegation in clones.
- Clones seeding GCs bifurcate into plasmablasts and exhibit isotype variegation.
- GC B cells accrue mutations at rates unaffected by anti-malarials.
- *Plasmodium* infection triggers antigen-independent Type I IFN-mediated bystander activation.
- B cell development is preserved in malaria by shifting from bone marrow to spleen.

Introduction

Antigen receptor engagement on naive B cells initiates not only clonal expansion, but also a range of phenotypic changes and genetic alterations that increases diversity beyond that offered by pre-existing BCRs alone. Phenotypes adopted include short-lived antibody-secreting plasmablasts, memory B cells, atypical B cells, germinal centre B cells and plasma cells, each with distinct functions within the overall humoral immune response. Further diversification proceeds via class switch recombination (CSR), which replaces the constant portion of BCRs with one of a number of functionally varied isotypes (*e.g.* IgG1, IgG2, IgG3, IgG4, IgA1, IgA2 and IgE in humans)[1,2]. In addition, B cells entering germinal centres (GC) can further diversify their BCRs via somatic hypermutation (SHM)[3-6], leading to affinity maturation of resulting antibodies[7].

B cell diversification during infection can either promote or impair humoral immunity, as evidenced during blood-stage *Plasmodium* infection, in which plasmablast responses can limit immunity to malaria[8], while increased breadth of antibody specifities[9,10] and effector functions[11] is associated with greater protection against symptoms. Understanding when diversification mechanisms operate and whether they interact *in vivo* may offer opportunities for tuning immunological responses.

Experimental vaccination with single antigens has revealed several *in vivo* aspects of CSR and phenotypic diversification in single naive B cells, in particular that CSR can occur early, prior to entry into the GC[12-14], that CSR occurs independently of phenotypic changes in some cases[15] but not others[16], and that the degree of phenotypic diversification by expanded clones is controlled by the BCR itself, and is further regulated by apoptosis during clonal expansion[15]. CSR is largely thought to act orthogonally to processes determining phenotypic fate, relying on stochastic expression of activation-induced cytidine deaminase (AID) and germ-line transcripts (GLT)[17]. Further experiments using viral infection have revealed SHM dynamics within the GC[18], showing that mutations accrue and then diminish in variable heavy chain regions due to invasion of GCs by naive B cells[18,19]. More recent single-cell transcriptomic studies performed on steady-state human tissues, has identified transient, intermediate states of B cell activation[20,21]. Although observations from viral infections and vaccination studies, and single-timepoint analyses of human tissues provide vignettes of B cell clonal diversification, the temporal relationships of, and interactions between these mechanisms remain to be determined within the context of a single *in vivo* model.

Here, we map over time the diversification mechanisms that operate in polyclonal B cells during infection with blood-stage *Plasmodium* parasites, an antigenically complex protozoan genus[22,23], which continues to pose a substantial threat to global human health[24]. To do so we employ scRNAseq, BCRseq, and spatial transcriptomics in conjunction with a mouse model of protective, $CD4^+$ T-cell dependent, antibody-mediated immunity.

Results

Plasmodium infection triggers contemporaneous B cell responses that vary in antigen-dependency.

To assess B cell clonal diversification over time, we employed blood-stage *Plasmodium chabaudi chabaudi* (*Pc*AS) infection of C57BL/6J mice. This model is characterised by peak parasitemia ~7-9 days post-infection, followed by $CD4^+$ T-cell dependent, antibody-mediated, parasite control over the following 60-90 days[25,26]. We performed paired scRNAseq and BCRseq of splenic polyclonal B cells ($CD19^+$ $B220^{int-hi}$) prior to and at 4-, 7-, 10- and 14-days post infection (dpi), reasoning this could capture early activation events and progressive emergence of plasmablasts and GC B cells (Fig. 1A). Combined data from replicate mice at each timepoint, analysed by dimensionality reduction, unbiased clustering, and canonical marker analysis, identified multiple subsets emerging over time (Extended Data Fig. 1A-C), in particular plasmablasts and GC B cells evident at days 10 and 14 dpi, displaying kinetics consistent with previous flow cytometric studies[25,26] (Fig. 1B), suggesting the utility of our scRNAseq data for examining antigen-dependent B cell diversification mechanisms *in vivo.*

In addition to expected, antigen-dependent B cell activation, our scRNAseq screen revealed that naive B cell transcriptomes diminished in frequency at 4 and 7 dpi, with an alternative cluster of unswitched, non-proliferating B cells emerging (Fig. 1C), defined by up-regulation of interferon-associated genes, including *Stat1*, *Socs1, Irf1* and *Irgm1* (Fig. 1D). *Ly6a* (encoding SCA-1) and *Ly6c2* (encoding Ly6C), were also upregulated (Extended Data Fig. 2A). This suggested B cells lacking specificity for *Plasmodium* antigens, had responded in a bystander, interferon-mediated fashion during infection. Kinetics of SCA-1 and Ly6C expression were confirmed at protein level on IgD^+ cells by 4 dpi, which was sustained until day 14, with SCA-1 remaining modestly elevated at 28 dpi (Fig. 1E). SCA-1/Ly6C up-regulation was still evident in CD4-depleted mice (Extended Data Fig. 2B)[25], indicating T-cell independence of this phenomenon. We confirmed bystander activation by assessing ovalbumin-specific OB1 cells after transfer and infection with non-ovalbumin expressing *Pc*AS (Fig. 1F; Extended Data Fig. 2C). Finally, SCA-1/Ly6C upregulation by IgD^+ cells was dependent on Type I IFN-signalling via IFNAR1 (Fig. 1G), while B cell-intrinsic genetic deficiency of the Toll-like receptor adaptor, *Myd88,* had no effect (Extended Data Fig. 2D). Thus, our scRNAseq screen revealed T-cell-dependent plasmablast and GC B cell differentiation had occurred amid antigen-independent Type I IFN-mediated bystander B cell activation in the spleen.

CSR overlaps with clonal expansion leading to isotype variegation amongst clones.

Next, given the emergence of plasmablasts and GC B cells within our transcriptomic dataset by 10-14 dpi (Fig. 1B), we hypothesized that early activation, clonal expansion and progressive phenotypic change might be detectable. We observed a transient increase at 4 dpi of cells marked by upregulation of *Myc, Nfkbid*, *Cd83, Cd69* and *Jun*, consistent with being early antigen-activated B cells[20,21,27-29] (Fig. 2A). Although we observed no cell-states consistent with intermediate or progressive differentiation towards plasmablasts, we did note adjacent positioning of GC B cells with early activated cells (Fig. 2A). Activated cells had not up-regulated cell-cycling genes (Fig. 2B). In addition, *Seurat* and Bayesian Gaussian Process Latent Variable Model (BGPLVM) embeddings suggested that CSR-related genes[20] were strongly expressed in early activated, non-cycling cells, as well as in emerging GC B cells (Fig. 2B). CSR-associated gene expression overlapped partially with *Myc* up-regulation and cell-cycle gene expression (Fig. 2B), suggesting temporal overlap of these processes. To examine this further, pseudotemporal ordering was performed after BGPLVM[30-32] (Fig. 2C). This placed *Myc*-upregulation as the earliest event in pseudotime, followed by CSR, and finally cell-cycling, with all signatures demonstrating partial overlap (Fig. 2C). Together, these data supported a model in which CSR initiates soon after *Myc* upregulation is triggered by cognate antigen, and importantly, then partially overlaps with clonal expansion. This raised the hypothesis, given our model induces IgG2b, IgG2c, IgG1 and IgG3, that clones exhibiting CSR prior to clonal

expansion would necessarily express a single IgG isotype, while those having undergone at least one cell division prior to CSR, could in theory exhibit isotype variegation. To test for variegation, we determined isotypes using parallel BCRseq data in clones at each timepoint post infection, focussing on 10 and 14 dpi, where clonal expansion was most evident (Fig. 2D). Cells were defined as clonal when sharing identical *V* and *J* genes, identical junctional CDR3 amino acid length, and >85% amino acid CDR3 sequence identity. Across expanded clones at 10 and 14 dpi from two independent experiments, 128 out of 528 expanded clones (25.9%) with 2 members exhibited isotype variegation (Fig. 2E). This rose to 50% for clonal families >2 (Fig. 2E), confirming that for many clones the progeny of a single naive B cell switches to more than one IgG isotype. Thus, our data supports partial temporal overlap between early CSR and subsequent clonal expansion in malaria.

B cell clones seeding GCs bifurcate into plasmablasts and exhibit isotype variegation.

We next tested whether phenotypic changes further contributed to the diversification of isotype variegated clones (Fig. 3A). Using BCRseq data combined with transcriptomic categorisation of phenotypes, across 16 mice from two independent experiments at days 10 and 14 dpi combined, we noted the majority of expanded clones detected gave rise only to plasmablasts (Fig. 3B, Extended Data Figs. 3-4), with 119 (25.8%) out of 460 clones exhibiting isotype variegation as described above (Fig. 3C). Of 92 expanded clones with 2 family members giving rise to at least one GC B cell, 53 (57.6%) had bifurcated to give rise to a plasmablast (Fig. 3C) – rising to 100% giving rise to plasmablasts for the small number of GC-containing clones with >2 family members (Fig. 3C). Importantly, of GC-containing clones with 2 family members ~20% exhibited both isotype variegation and phenotypic diversity (Fig. 3C). Together, these data highlighted during the first two weeks of infection a spectrum of clonal diversification outcomes within the GC, with many clones exhibiting both phenotypic diversification and isotype variegation.

GC B cells retain diversity and a constant SHM rate during infection and anti-malarial treatment.

We next tested whether SHM further diversified GC B cells during prolonged parasitic infection, contrary to previous reports highlighting reduced affinity maturation and disrupted splenic GC structures in individuals living in malaria-endemic regions[33,34]. We assessed an extended scRNAseq time course until 42 dpi, which included an experimental arm to determine effects of anti-malarial drug intervention from 7 dpi, which as expected, accelerated parasite removal in our system (Fig. 4A, Extended Data Fig. 5A).

To enrich for B cells activated via cognate antigen, we FACS-sorted IgD^{lo} B cells ($CD19^{+}$ $B220^{int-hi}$), spiking back in small numbers of IgD^{hi} naive cells at each scRNAseq timepoint to assist in removal of batch effects. After combining data across all timepoints, treatments, and mice as above (including confirmation of minimal batch effects via IgD^{hi} spike-in assessment), we inferred 11 distinct cell types (Fig. 4B), most of which showed little to no change in frequency as a result of anti-malarial treatment, except for MZ B cells and B1 cells, which increased by 148% and 75%, respectively, while GC B cells dropped by 36.2% (Extended Data Fig. 5B). Distinct dynamics existed for some cell-types, including a drop-off in antibody secreting cells (ASCs) by 21 dpi, and a gradual increase in GC B cells (Fig. 4B and Extended Data Fig. 6A-B), with atypical and memory B cells relatively constant over time. By 42 dpi GC B cells had become a major subset (Fig. 4B). Further phenotypic characterisation of GC B cell subsets using canonical gene markers and gene signatures[35], identified putative Light Zone (LZ), Dark Zone proliferating (DZp) and differentiating (DZd) cells, as well as mixed LZ/DZ cells. Further evidence of these as distinct subsets was provided by spatial transcriptomics, which localised LZ and DZp/DZd transcriptomes to adjacent microanatomical regions within GCs in the spleen at 30 dpi[32] (Fig. 4C). Over the time course, LZ cells became a smaller fraction of the GC, which stabilised by 21 dpi, while DZd cells similarly increased and plateaued over the same time period, with DZp cells remaining relatively constant (Fig. 4C). These data suggested an equilibrium had been reached at a population level. Of note, elevation in LZ cells

between 10-14 dpi was abrogated by anti-malarial intervention, suggesting circulating parasite burden had supported early LZ reactions within the GC (Fig. 4C). Nevertheless, the effect of anti-malarials on GC composition was transient, with an apparent equilibrium reached by 42 dpi (Fig. 4C). Evidence of GC functional stability was provided by *Aicda* gene expression, strongly expressed as expected in DZ GC B cells (Fig. 4D), and most importantly, stably expressed over the course of infection with or without anti-malarial drug treatment (Fig. 4E). This raised the hypothesis that acquisition of mutations within GCs occurred at a constant rate refractory to anti-malarial treatment. To test this, we compared BCR sequences to germline, and detected, as expected, few mutations in BCRs of either naive follicular B cells or subsets not expected to engage in SHM (Extended Data Fig. 7). Consistent with our hypothesis, GC B cells exhibited a progressive increase in the median number of mutations summed across heavy and light chains, at a rate of 3.71 mutations per week, which remained unaltered (3.79 mutations per week) upon exposure to anti-malarials (Fig. 4F and Extended Data Fig. 8A). However, contrary to our hypothesis that later stage GCs harbour only highly mutated BCRs, the interquartile range of GC mutation counts increased over time (Extended Data Fig. 8B), such that by 42 dpi GCs harboured BCRs exhibiting a spectrum of mutations from 0-40 mutations per cell.

SHM rates observed in this study were similar to those calculated from previous studies of Ighv regions of murine lymph node GC B cells after influenza infection[18,36] (Extended Data Fig. 8C), suggesting that SHM during infection with *Plasmodium* was not impaired relative to that induced during viral infection. Finally, we sought to determine how increase in diversity of mutation count within GCs related to diversity in antibody isotype (Fig. 4F). Firstly, there was no clear skewing of highly mutated BCRs towards IgG1, IgG2b, IgG2c, IgG3 or IgA (Fig. 4F). Most notably, there remained over the time course, either with or without anti-malarial intervention, a proportion of GC B cells that were IgM^+ and harboured 0-10 mutations (Fig. 4F and Extended Data Fig. 9). These data revealed that GC B cells with low numbers of mutational counts were heavily skewed to IgM, while highly mutated BCRs had switched to IgG isotypes. Taken together, our data reveal a constant rate of SHM-mediated diversification of GC B cells during *Plasmodium* infection, further diversified by the emergence and retention of unswitched cells with low mutation counts.

Anti-malarial treatment impairs GC output during experimental malaria.

Although GC microanatomy, GC B cell diversity, and SHM rates appeared unaffected by treatment with anti-malarials, there was nevertheless an apparent drop in GC B cell frequency as a result of drug intervention (Extended Data Fig. 5B), which suggested a quantitative effect on GC responses. Hence, we hypothesized that GC output might be affected by anti-malarial treatment. Inferred switched memory and atypical memory B cells, which had acquired mutations in BCRs consistent with GC origin (Extended Data Fig. 10), were largely unaltered in frequency in our scRNAseq data (Extended Data Fig. 5B) after anti-malarial treatment, suggesting no major effect on memory B cells emerging from GCs.

Instead, we sought to assess emerging plasma cells in the spleen by isolating and re-clustering ASC transcriptomes from our scRNAseq data of IgD^{lo} $CD19^+$ $B220^{int-hi}$ cells (Fig. 5A). This highlighted a cluster highly-expressing *Prg2,* a marker of splenic plasma cells[37] (Fig. 5A). *Prg2*^{hi} ASCs were predominantly isotype switched (Fig. 5B), and harboured high mutation counts from 21 dpi (Fig. 5C), consistent with being emerging splenic plasma cells. Importantly, *Prg2*^{hi} ASCs significantly dropped in frequency (Fig. 5D), although with limited evidence of a drop in mutation count (Fig. 5C), after anti-malarial treatment, suggesting a quantitative drop in plasma cell output from GCs. Consistent with this, anti-malarial drug treatment reduced circulating parasite-specific IgG (Fig. 5E), and rendered mice more susceptible to high parasite burdens after high-dose homologous re-challenge (Fig. 5F). Taken together, our data reveal that anti-malarial treatment exerts quantitative limits on the development of splenic plasma cells from the GC.

B cell lymphopoiesis relocates to the spleen during experimental malaria.

The presence of IgM$^+$ GC B cells with low mutation counts at 21-42 dpi prompted us to hypothesise these as recently activated B cells invading established GCs. In considering ongoing sources of naive B cells, we noted from 14 dpi, the emergence of cells lacking *Ighd* expression, and expressing *Il7r* and surrogate light chain gene *Vpreb1,* consistent with annotation as precursor B cells (Extended Data Fig. 1C and 6A). Next, we integrated our independent scRNAseq datasets into a combined UMAP (Extended Data Fig. 11A-C) and tested for presence of developing B cells by integrating with a publicly available scRNAseq dataset of developing B cells in the bone marrow[38] (Fig. 6A and Extended Data Fig. 11D). Our splenic data merged with the bone marrow dataset in certain expected areas, *e.g.* mature B cells (cluster 1) and plasma cells (cluster 13) (Fig. 6A). Next, our inferred splenic immature and precursor B cell populations integrated closely with reported bone marrow counterparts (Fig. 6A). Based on the integrated embedding and canonical markers, we annotated precursor B cells as pro-and cycling pro-B cell (*Vpreb1, Igll1, Dntt, Rag1, Il7r, Il2ra, Ebf1, Ighd$^-$, Cd74$^-$, Ms4a1$^-$*), pre-B cells (*Rag1, Il7r, Il2ra, Ebf1, Ighd$^-$, Cd74$^-$, Ms4a1$^-$)* and immature B cells (*Ighd$^-$, Ighm$^+$, Ms4a1, Cd74*) (Fig. 6B and Extended Data Fig. 11E). Mapping these over time revealed pro- and cycling pro- B cells emerged first at 14 dpi, before subsiding, followed by pre-B cells peaking at 21 dpi, with immature B cells persisting until the end of the experiment (Fig. 6B). Anti-malarial drug treatment had no major effects on these dynamics (Fig. 6B). We confirmed these dynamics via flow cytometric analysis of IL7R, IgM, CD43 and CD24 expression on IgD^{lo} CD93$^+$ non-plasmablast, non-GC B cells (Fig. 6C and Extended Data Fig. 11F), revealing that extramedullary B cell lymphopoiesis had occurred in this model. Finally, assessment at 30 dpi of the relative location of multiple cells types via spatial transcriptomics and deconvolution using scRNAseq reference data, as previously reported[32], revealed immature B cells localising within B cell follicles (Fig. 6D and Extended Data Fig. 12), suggesting their capacity to give rise to mature, naive B cells. Thus, taken together, our data revealed that during experimental malaria, B lymphopoiesis occurs in the spleen in parallel with GC responses (Fig. 6E), that it persists for substantial periods of time, and likely gives rise to mature, naive B cells within follicles.

Discussion

In this study we tested the hypothesis that population-level diversity in the phenotypes and antibody sub-classes adopted by polyclonal B cells during infection is partly mediated by intra-clonal diversity. We chose to study experimental malaria, rather than single-antigen vaccination, because *Plasmodium* parasites express hundreds of proteins[22,23], and might be predicted to activate a broad spectrum of antigen-specific B cell clones. Furthermore, immunity to malaria is contingent on effective production of *Plasmodium*-specific antibodies[39]. By employing scRNAseq and paired BCRseq over time, we observed it was commonplace amongst hundreds of expanded clones, for the progeny of single naive B cells to vary both in terms of the phenotypes and the switched IgG sub-classes adopted. This suggests that during infection with a complex pathogen, although initial BCR sequence and antigen affinity can determine fate, as with single-antigen vaccination[15], that BCR-independent processes may also be important for diversifying the progeny of single naive B cells.

CSR can occur early during experimental vaccination, prior to GC formation[12-14]. Our observations during *Plasmodium* infection are consistent with this model, although the absolute timing of responses appears slower than that elicited by vaccination, perhaps due to low parasite numbers and hence antigen availability at early stages. scRNAseq over time facilitated the inference that *Myc*-upregulation, CSR and clonal expansion occur in a specific order, that nevertheless overlap temporally with each other. The consequences of overlap between clonal expansion and CSR is that certain clones might switch prior to clonal expansion, while others would expand before switching. Our data is consistent with this, since some clones but not others displayed isotype variegation. To determine whether intra-clonal phenotypic variation is beneficial one might consider an alternative scenario in which initial BCR-sequence fully determines fate and isotype in a given innate immune environment. In such a case, clones displaying specificity for an important, protective, parasite-derived epitope would be locked into a single response that may or may not be optimal for pathogen control. In contrast, intra-clonal diversity early during infection may act as a “bet-hedging” strategy, providing clones with functional flexibility, *e.g.* to enter the GC or not, to produce IgG2b, IgG3 or IgG2c, or to elicit rapid extra-follicular responses. Since many initial GC clones had also given rise to plasmablast fates, we hypothesise that most clones have a capacity to seed a nascent GC, making it an inclusive process. This would provide a wide range of antigen-specificities the opportunity to increase affinity for *Plasmodium* epitopes, with the exception of certain BCRs which might skew towards a plasmablast fate.

Data from this study, together with previous reports[12-14], prompts a consideration of why CSR initiates early, prior to GC entry. One explanation is that innate cytokine-mediated tailoring of humoral immune responses[40-42], specifically of which antibody isotypes to deploy for a given pathogen class, must necessarily occur soon after pathogen sensing has occurred, *e.g* via pathogen-associated molecular patterns (PAMPs). This is likely to be within hours to a few days after pathogen exposure. Hence, it seems likely CSR must be initiated at a time when innate immune responses have recently occurred, and innate cytokines are circulating within secondary lymphoid organs. Additionally, it may streamline affinity maturation within the GC by having many clones switched to IgG early during infection. Of note, this model does not preclude CSR from continuing within the GC, a prominent zone for AID expression[43,44]. Given the persistence of IgM^+ GC clones in our model as in other studies[14,45], we speculate that CSR continues in the GC across various times during infection.

The initial dynamics of SHM within GCs have been explored during hapten exposure or viral infection[18,36,46]. This has revealed linear rates of mutation acquisition in the heavy chains of BCRs ranging from 1.9-2.1 mutations per week[18,36]. In our model, we also note a constant SHM rate over the first 6 weeks of infection of ~2 mutations in the heavy chain per week, with similar rates evident for light chains. Our analysis suggests firstly, that SHM occurs during protozoan parasitic infection at a rate that is comparable to, if not higher than, that induced during viral infection[18,36]. Although

our previous work, and others have revealed GC B cell responses are sub-optimal during *Plasmodium* infection[25,26], we hypothesise this is due to limits on clonal expansion and fate choice, rather than adverse effects on SHM rate. Secondly, we consider why the rate of SHM is constant. Given that AID expression levels are constant in GC B cells over time in our model, we hypothesize a constant mutational clock operates in GC B cells, governed predominantly by AID levels present per cell. Thirdly, consistent with the concept of a constant mutational clock, we noted that anti-malarial treatment, which lowers parasite numbers and protects against splenomegaly, had no effect on SHM rates, despite deleterious effects on GC size, antibody titres and plasma cell differentiation. The clinical significance of our findings may be that humans treated for mild malaria symptoms with anti-malarials[24] could nevertheless harbour GCs in which affinity maturation can continue. Whether sufficient antigen is present on follicular dendritic cells (FDCs) to facilitate selection after anti-malarial treatment remains to be determined.

Finally, our non-targeted approach of examining polyclonal B cells facilitated the discovery of two phenomena that would have been missed with a focus on antigen-specific cells: Type I IFN-mediated bystander B cell activation, and the developmental pathway for extramedullary, or “emergency” B cell lymphopoiesis. Both these processes occurred contemporaneously, and in the same organ as antigen-specific B cell differentiation. Although our previous work indicated that IFNAR1-signalling via conventional dendritic cells impaired the onset of T-cell dependent humoral immunity[25], the significance of Type I IFN-effects on antigen-irrelevant B cells remains unclear at present. We speculate that immune-regulatory networks, perhaps controlled by Suppressor of Cytokine Signalling (SOCS) proteins may restrain bystander B cells. Whether there are longer-term effects on bystander B cells during future immune challenges remains to be determined.

It has been reported previously that *Plasmodium* infection can profoundly affect haematopoiesis in the bone marrow, with clear consequences for myelopoiesis[47,48]. Common lymphoid progenitors are detected in adult mouse spleen[49], with one study also suggesting these could undergo B cell development during *Plasmodium* infection[50]. Our study reveals that various immature forms of B cells are readily detected in the spleen during malaria, and that the classical developmental pathway of pre-B cells, pro-B cells and immature B cells in the bone marrow is likely phenocopied in the spleen, with spatial transcriptomic assessment suggesting immature B cells re-populate B cell follicles. We also reveal the potential for IL7R to act as a marker for developing B cells in the spleen. Our findings support the hypothesis that emergency B cell lymphopoiesis in the spleen in malaria serves to fuel persisting GCs.

In summary, we have identified multiple biological phenomena within splenic B cells during infection with blood-stage *Plasmodium* parasites. Amid a backdrop of bystander activation, single naive B cells with initial specificity for parasites proliferate and exhibit a spectrum of intra-clonal functional diversification. This diversity is maintained, and increased in the GC with a constant rate of SHM, and persistence of switched and unswitched GC B cells throughout infection and treatment. Finally, deleterious effects on B cell development in bone marrow[51] are counteracted by relocating this process to the spleen, potentially allowing the body to respond to ongoing or future immunological challenges.

Limitations

Although our temporal assessment of polyclonal B cells aimed to capture the transition of B cells from one state to another, we were unable to identify an intermediate state between activated B cells and plasmablasts. This may have been due to the relative sparsity of timepoints at early stages of the immune response, rather than there being a lack of such an intermediate state. Secondly, the reduced capacity to detect BCR sequence data for GC B cells compared to plasmablasts prevented us from making unequivocal statements around the probabilities and frequencies with which naive B cells opted for these two fates. Rather, we restricted our conclusions to whether or not single clones giving rise to GC B cells could bifurcate into plasmablasts. Thirdly, our FACS-sorting strategy would not have isolated long lived plasma cells (LLPCs), meaning that plasma cell output from the GC could not be comprehensively assessed[52]. Instead, we infer *Prg2*-expressing ASCs in the spleen[37] were likely emerging or early-stage PCs, yet to down-regulate CD19 as described by others[53]. Finally, our scRNAseq assessment of tens of thousands of polyclonal cells identified a relatively small range of clone sizes, with the largest clone comprised of 9 cells. This is in contrast to other studies where enrichment of antigen specific B cells from entire organs can identify the full clonal size information, albeit against one type of antigen[15]. Future studies examining 100-1000 fold more polyclonal B cells per spleen will enable a fuller analysis of the relationship between antigen-specificity and clone size.

Methods

Mice

C57BL/6J mice were sourced from Animal Resources Centre (Perth, Western Australia, Australia) maintained under specific pathogen-free (SPF) conditions within the Biological Research Facility (BRF) of The Peter Doherty Institute for Infection and Immunity (Melbourne, Victoria, Australia). Mice were housed at an ambient air temperature of 19-22ºC, at 40-70% humidity with a 12-hour day/night cycle. OB1.*Rag*−/−.uGFP and CD23Cre-MyD88flox were bred in-house in the BRF of The Peter Doherty Institute for Infection and Immunity and maintained under the same conditions described above. Unless stated otherwise, all experimental mice used were female mice at 6-12 weeks old. All animal procedures were approved by the University of Melbourne Animal Ethics Committee (1915018).

Adoptive transfer

Uninfected spleens from OB1.*Rag*−/−.uGFP female donor mice were collected and homogenised through 70µM cell strainers. Homogenates were incubated with red blood cell (RBC) lysis buffer (Pharm Lyse, BD) for 3 minutes at room temperature. Each C57BL/6J recipient mice received $15x10^6$ OB1 cells by lateral tail vein injection in a volume of 200µl.

Infection

Passage C57BL/6J mice were infected with a thawed vial of *Plasmodium chabaudi chabaudi* clone AS (*Pc*AS) infected RBC stabilite. Once parasitemia reached 1-5%, blood was collected from passage mice by intra-cardiac bleed into RPMI containing 5U/ml heparin. A total of 10^5 parasitized RBCs were injected into each experimental mouse via lateral tail vein injection. For rechallenge, mice were infected with 10^7 parasitized RBCs via lateral tail vein injection, 28 days after primary infection with *Pc*AS.

Parasitemia assessment

Parasitemia measurements were carried out as described previously[26]. Briefly, tail vein bleeds were performed to collect a drop of blood into RPMI containing 5U/ml of heparin. Diluted blood samples were stained at room temperature, for 30 minutes in the dark, with a combination of Hoechst 33342 (10µg/ml; Sigma-Aldrich) and Syto84 (5µM; Life Technologies). Cold RPMI was used to quench the staining with 10 times initial volume. The percentage of parasitized RBCs were determined as the proportion of Hoechst$^+$ Syto84$^+$ RBCs assessed using a Fortessa cytometer (BD).

Anti-malarial drug treatment

Artesunate (Guilin Pharmaceutical, kindly gifted by J. Mohrle) was made to 50mg/ml in 5% sodium bicarbonate solution (in PBS) and diluted with 0.9% saline (Baxter) to form a 5mg/ml solution of sodium artesunate. From day 7 post malaria infection, 1mg of sodium artesunate was injected intra-peritoneally twice daily to day 9, then once a day from day 10 to day 16 and twice weekly from day 17 to day 42 post malaria infection, alternating left and right side per i.p. injection. Additionally, from day 7 until day 42, mice received 70mg/l of pyrimethamine (Sigma Aldrich) in the drinking water.

CD4+ T cell depletion

At 4 days prior to *Pc*AS infection, mice were administered 0.2mg of anti-CD4 depleting monoclonal antibody (clone GK1.5, BioXcell) or isotype control antibody (clone LTF-2, BioXcell) and a further 0.1mg dose was administered one day prior to infection. Antibodies were administered by intra-peritoneal injection in 200µl sterile PBS.

IFNAR blockade

On the day of *Pc*AS injection, prior to infection, mice were administered 0.1mg of anti-IFNAR1 monoclonal antibody (clone MAR1-5A3, Leinco) or isotype control antibody (clone HKSP84, Leinco) and a further 0.1mg dose day 2 post infection. Antibodies were administered by intra-peritoneal injection in 200µl sterile PBS.

IV Label

To differentiate between lymphocytes that are in circulation and those that are within tissue, prior to spleen isolation, the mice were labelled with CD45.2 (clone 104, BioLegend) fluorescently conjugated antibody. A total of 15µl CD45.2-APC antibody was made up to 200µl in sterile 1x PBS and administered to each mouse via lateral tail vein injection. After 5 minutes, mice were culled and spleens harvested. With this strategy, CD45.2^{-} lymphocytes will be intravenous label negative (IV^{-}) and are inferred as more tissue residing, as opposed to circulating lymphocytes (that would stain positively for CD45.2).

Flow cytometry

After spleen homogenisation through 70µM cell strainers and red blood cell lysis using Pharm Lyse (BD), cells were stained with Zombie Yellow live/dead stain (BioLegend) (1:500) in PBS on ice for 15 minutes, followed by Fc receptor block (BD) in FACS wash buffer (2% FCS, 1mM EDTA in PBS) on ice for 20 minutes. Finally, cells were stained with different titrated panels of monoclonal antibodies diluted in FACS wash buffer (refer to table for antibody details). For intracellular staining, surface-stained cells were fixed and permeabilised using FoxP3/Transcription Factor Staining Set (eBiosciences) then stained with titrated antibody panels for 20-30 minutes on ice in the dark. Cells were acquired using Fortessa cytometer (BD), with all analysis of raw data performed using FlowJo version 5 (Treestar). Fluorescence minus one (FMOs) for SCA-1, Ly6C, IgM and IL7R were used to help draw gates for each marker.

Marker	Fluorophore	Clone	Source	Titration	Surface/ICS
B220	AF700	RA3-682	BioLegend	1:200	Surface
B220	BUV395	RA3-6B2	BD	1:200	Surface
CD19	PE-Cy7	6D5	BioLegend	1:200	Surface
CD19	PerCP-Cy5.5	1D3/CD19	BioLegend	1:200	Surface
CD19	FITC	6D5	BioLegend	1:200	Surface
CD24	PE-Cy7	M1/69	BioLegend	1:200	Surface
CD38	BUV737	90/CD38	BD	1:200	Surface
CD43	AF700	S11	BioLegend	1:100	Surface
CD86	PE-Cy7	GL1	BD	1:200	Surface
CD93	PE	AA4.1	BioLegend	1:200	Surface
CD95/Fas	PE-CF594	Jo2	BD	1:200	Surface
CD127/IL7R	BV421	A7R34	BioLegend	1:200	Surface
CD138	BV786	281-2	BD	1:100	Surface
IgD	BV711	11-26c-2a	BioLegend	1:200	Surface
IgM	APC-Cy7	RMM-1	BioLegend	1:100	Surface
Ly6a/SCA-1	APC-Fire	D7	BioLegend	1:100	Surface
Ly6c	PE	HK1.4	BioLegend	1:100	Surface
TCRβ	BUV737	H57-5797	BD	1:200	Surface

Detection of parasite-specific serum antibodies by ELISA

Serum was collected from uninfected and infected mice (day 55-60 post-*Pc*AS) with or without anti-malarial drug treatment and diluted 1/400, 1/800, 1/1600 or 1/3200 to assess binding to crude antigen extracts from *Pc*AS-infected pRBCs, as previously described[54].

Cell sorting and scRNAseq

Spleens were harvested from mice and homogenised through 70µM cell strainers. RBCs were lysed using Pharm Lyse (BD) for 3 minutes at room temperature and then single cell suspensions washed twice in 1x PBS. Samples were then incubated with Fc receptor-blocking antibodies (BD) for 20 minutes on ice, followed by incubation with titrated monoclonal fluorescently conjugated antibodies and TotalSeq-C (BioLegend) mouse hashtags for 20 minutes on ice. Cells were washed twice and resuspended with propidium iodide (1:500 dilution) in PBS 2% BSA.

For experiment 1, samples from five individual mouse replicates were pooled together for each timepoint. Note, for timepoint day 4 post infection, there were four separately infected mice with one uninfected naive sample pooled in. Live, TCRβ negative, $CD19^{+}$, $B220^{int\text{-}hi}$ cells were sorted using a FACS Aria III (BD) into a 2% BSA/PBS buffer. For experiment 2, samples from seven individual mice (three for *Pc*AS, three for *Pc*AS+drug and one uninfected) were pooled together for each timepoint. Live, TCRβ negative, CD19+, $B220^{int\text{-}hi}$, IgD^{lo} cells were sorted using a FACS Aria III (BD) into a 2% BSA/PBS buffer. For each sample, a small number of IgD^{hi} naive cells were spiked in to assist in removal of batch effects for downstream scRNAseq analysis.

After sorting, cells were loaded onto the chromium controller and using the Chromium GEM-X Single Cell 5' Kits v3 (Catalogue #1000695;10X Genomics), cDNA-sequencing libraries were prepared.

Analysis of scRNAseq datasets

For both the experiment 1 (days 0-14) and experiment 2 (days 10-42), the transcriptome of splenic B cells was aligned using Cell Ranger 3.1.0 (10X Genomics) against mouse genome v2020-A (10X Genomics). Hashtag demultiplexing and pre-processing of the data was performed using R version 4.2.0 and Seurat version 4[55]. Doublets and negatives were removed from the demultiplexed samples for further downstream analysis (Supplementary Method Fig. 1A and 2A). For pre-processing, cells with a mitochondrial gene content of greater than 10% were removed as well as cells with fewer than 200 and greater than 6000 total gene expression (Supplementary Method Fig. 1B and 2B).

Normalisation of data, selection of highly variable features and scaling of data were achieved using the *SCTransform()* function using default settings. Dimensional reduction was performed using the *RunPCA()* function and the resultant principal components were inputted to perform unifold manifold approximation and projection (UMAP) using *RunUMAP()* function. Finally, *FindNeighbours()* function and *FindClusters()* functions were used for unsupervised clustering.

Additionally, if immunoglobulin genes were left in the dataset for high dimensional reduction and clustering, clusters formed based purely on certain immunoglobulin variable heavy or light chain regions (Supplementary Method Fig. 1C and 2C). Therefore, immunoglobulin related genes (list of genes in Supplementary Table 1) were removed from the high dimensional reduction and clustering analysis, as recommended previously[56]. After high dimensional reduction and clustering analysis, UMAPs of each experiment were generated which highlighted anomalous cell clusters in each dataset: high mitochondrial content clusters, monocytes (*Lyz2*) and additionally in experiment 2, T cells (*Cd3g*) and erythrocytes (*Hbb-bs*) (Supplementary Method Fig. 1D and 2D). These clusters were removed from the UMAPs for subsequent downstream analysis. Altogether, after these quality control approaches, there were a total of 112,982 B cells: 40,623 B cells from experiment 1 and 72,359 B cells from experiment 2.

Cell type annotation

Differential gene expression analysis was performed using the *FindMarkers()* function with Wilcoxon rank sum test used to identify statistically significant differentially expressed genes across clusters. Geneset enrichment analysis (GSEA) was performed against biological processes GO terms using ToppGene Suite[57] or WebGestalt[58]. Gene signatures were sourced from publicly available datasets for the following signatures: cell cycle[59], class switch recombination (CSR)[20], GC B cell subsets[35] and B1a cells[60]. These cluster gene lists in addition to GSEA analysis and gene signatures aided in cell annotation of clusters for each UMAP.

Sub-clustering

To further sub-cluster ASC and GC B cell subsets, each subset were taken separately and the above workflow repeated, i.e. normalisation, *SCTransform(), RunPCA(), RunUMAP(), FindNeighbours()* and *FindClusters().*

Data integration

Single-cell variational inference (scVI)[61] was used to account for batch effects when performing data integration of day 10-42 B cell dataset with publicly available scRNAseq data of bone marrow B cells[38]. All parameters were kept at default and number of epochs set to 30 to train the model. Latent variables were used as input to run UMAP using *Scanpy* package (v1.9.1)[62]. In addition, data integration was performed on experiment 1 and 2 B cell datasets to generate a combined scRNAseq B cell dataset using the above parameters but using 9 epochs to the train the integration model.

Bayesian Gaussian Process Latent Variable Model (BGPLVM)

Pseudo-temporal ordering of activated and GC B cells was performed using Bayesian Gaussian Process Latent Variable Model (BGPLVM) using *GPFates*[30]. This generated a progression of activated and GC B cell transcriptomes that correlated with sampled timepoints as well as an inferred pseudotime trajectory.

Spatial transcriptomics using *Slide-seqV2*

Spatial transcriptomics was performed using *Slide-seqV2* at the Broad Institute of Harvard and MIT, as described elsewhere[63]. The methodology for the following spatial transcriptomic datasets were performed as previously described[32,64].

Spatial deconvolution was achieved using robust cell type decomposition (RCTD) algorithm on day 30 *Pc*AS infected spleens with artesunate treatment[65] (n=4, two spatial transcriptomic arrays per spleen for two infected mice). The single cell transcriptomic references used were from the day 10-42 B cell dataset, using all B cells from day 21, 28 and 35 artesunate treated mice and using GC B cells subsets from all timepoints and conditions. In addition, our reference contained CD4, CD8 T cells, NK cells, macrophages, monocytes, erythrocytes, granulocytes, cDC1s, cDC2s and pDCs from an uninfected spleen reference dataset[64]. Finally, our reference contained cells from a publicly available spleen stromal dataset from uninfected mice, which included fibroblastic reticular cells (FRCs), follicular dendritic cells (FDCs), red pulp reticular cells (RPRCs) and adventitial reticular cells (ARCs)[66].

BCR sequencing and analysis

Dandelion package[67] was used for VDJ clonal analysis.

Pre-processing

Using Dandelion, the data was pre-processed using the standard outputs from all cellranger vdj versions. Here, single-cell V(D)J data from the 5′ Chromium 10X kit were initially processed with cellranger vdj pipeline (v6.1.2). BCR contigs contained in 'all_contigs.fasta' and 'all_contig_annotations.csv' files were then re-annotated using an immcantation-inspired pre-processing pipeline contained in the Dandelion singularity container (v0.3.0).
The pre-processing pipeline includes the following steps:

i. Adjust cell and contig barcodes by adding user-supplied suffixes and/or prefixes to ensure that there are no overlapping barcodes between samples.
ii. Re-annotation of contigs with igblastn (v1.19.0) against IMGT (international ImMunoGeneTics) reference sequences.
iii. Re-annotation of *D* and *J* genes separately using blastn with similar parameters as per igblastn (dust = 'no', word size (J = 7; D = 9)) but with an additional *e*-value cutoff (J = 10^{-4} in contrast to igblastn's default cutoff of 10; D = 10^{-3}). This is to enable the annotation of contigs without the *V* gene present.
iv. Identification and recovery of nonoverlapping individual *J* gene segments (under associated 'j_chain_multimapper' columns). In the list of all mapped *J* genes (all_contig_j_blast.tsv) from blastn, the *J* gene with the highest score (j_support) was chosen. Dandelion then looks for the next *J* gene with the highest 'j_support' value, and with start (j_sequence_start) and end (j_sequence_end) positions not overlapping with the selected *J* gene, and does so iteratively until the list of all mapped *J* genes are exhausted. In contigs without *V* gene annotations, it then selects the 5′ end leftmost *J* gene and update the 'j_call' column in the final AIRR table. For contigs with *V* gene annotations, but with multiple *J* gene calls, it uses the annotations provided by igblastn.

For BCRs, there are two additional steps:

i. Additional re-annotation of heavy-chain constant (C) region calls using blastn (v2.13.0) against curated sequences from CH1 regions of respective isotype class.
ii. Heavy chain *V* gene allele correction using TIgGER (v1.0.0). The final outputs are then parsed into AIRR format with change-o scripts.

The rearrangement sequences that pass standard quality control checks are saved in file ending with the suffix '_contig_dandelion.tsv'.

Postprocessing

In addition to the pre-processing steps at the contig level, postprocessing or integrating cell-level quality control is performed using Dandelion's 'check_contig' function. The function checks whether a rearrangement is annotated with consistent *V*, *D*, *J* and *C* gene calls and performs special operations when a cell has multiple contigs. All contigs in a cell are sorted according to the unique molecular identifier (UMI) count in descending order, and productive contigs are ordered higher than non-productive contigs. For cells with other than one pair of productive contigs (one VDJ and one VJ), the function will assess if the cell is to be flagged with having orphan (no paired VDJ or VJ chain), extra pair(s) or ambiguous (biologically irreconcilable, for example, both BCRs in the same cell) status with an exception that IgM and IgD are allowed to coexist in the same B cell if no other isotypes are detected. The function also asserts a library type restriction with the rationale that the choice of the library type should mean that the primers used would most likely amplify only relevant sequences to a particular locus. Therefore, if there are any annotations to unexpected loci, these contigs likely represent artifacts and will be filtered away. A more stringent version of 'check_contigs' is used here by a separate function, 'filter_contigs', which only considers productive VDJ contigs, asserting a single cell should only have one VDJ and one VJ pair, or only an orphan VDJ chain, and explicitly removes contigs that fail these checks (with the same exceptions for IgM/IgD as per above). Productive contigs are selected for downstream analysis (Supplementary Methods Fig. 3A-

B). Summary of frequency of unexpanded and expanded clones for each timepoint and experiment can be found in Supplementary Method Fig. 3.

Clonotype definition and diversity

BCRs are grouped into clones/clonotypes based on the following sequential criteria that apply to both heavy-chain and light-chain contigs as follows:
(1). Identical *V* and *J* genes usage
(2). Identical junctional CDR3 amino acid length and
(3). CDR3 sequence similarity for BCRs is to use 85% amino acid sequence similarity (based on Hamming distance).

Somatic Hypermutation (SHM)

The basic mutation load is quantified by using the 'pp.quantify_mutations' in Dandelion which is a wrapper of SHaZam's basic mutational analysis. It sums all mutation scores (heavy and light chains, silent and replacement mutations) for the same cell.

GC B cell mutation analysis

Mutation rate analysis is calculated by fitting linear regression line to the median number of mutations at each timepoint for each condition (*Pc*AS or *Pc*AS+drug). The gradient of the line provides the mutation rate per day. Mutation rate analysis was also performed specifically on the Ighv region of the BCR in comparison with publicly available clonal data from lymph node GC B cells after influenza infection[18,36].

Plotting

For data visualisation, the following packages were used: Prism version 9, Tableau (2023.2.0), Python version 3.8.8 or ggplot2 version 3.4.4 package utilised in R version 4.2.1. Adobe Illustrator version 26.3.1 was used for figure generation and schematics were partly generated using BioRender.

Acknowledgements

This research was supported by The University of Melbourne's Research Computing Services, the Petascale Initiative, and the LIEF HPC-GPGPU Facility hosted at The University of Melbourne. The facility was established with the assistance of LIEF grant LE170100200. We extend our gratitude to the Biological Research Facility located at The Peter Doherty Institute for Infection and Immunity for their animal care and assistance. We also thank the Doherty Institute node of the Melbourne Cytometry Platform at The University of Melbourne. We would also like to acknowledge Dr Katherine Jackson (Garvan Institute of Medical Research, Sydney, Australia) for discussions and help regarding BCR sequencing analysis.

Main Figures

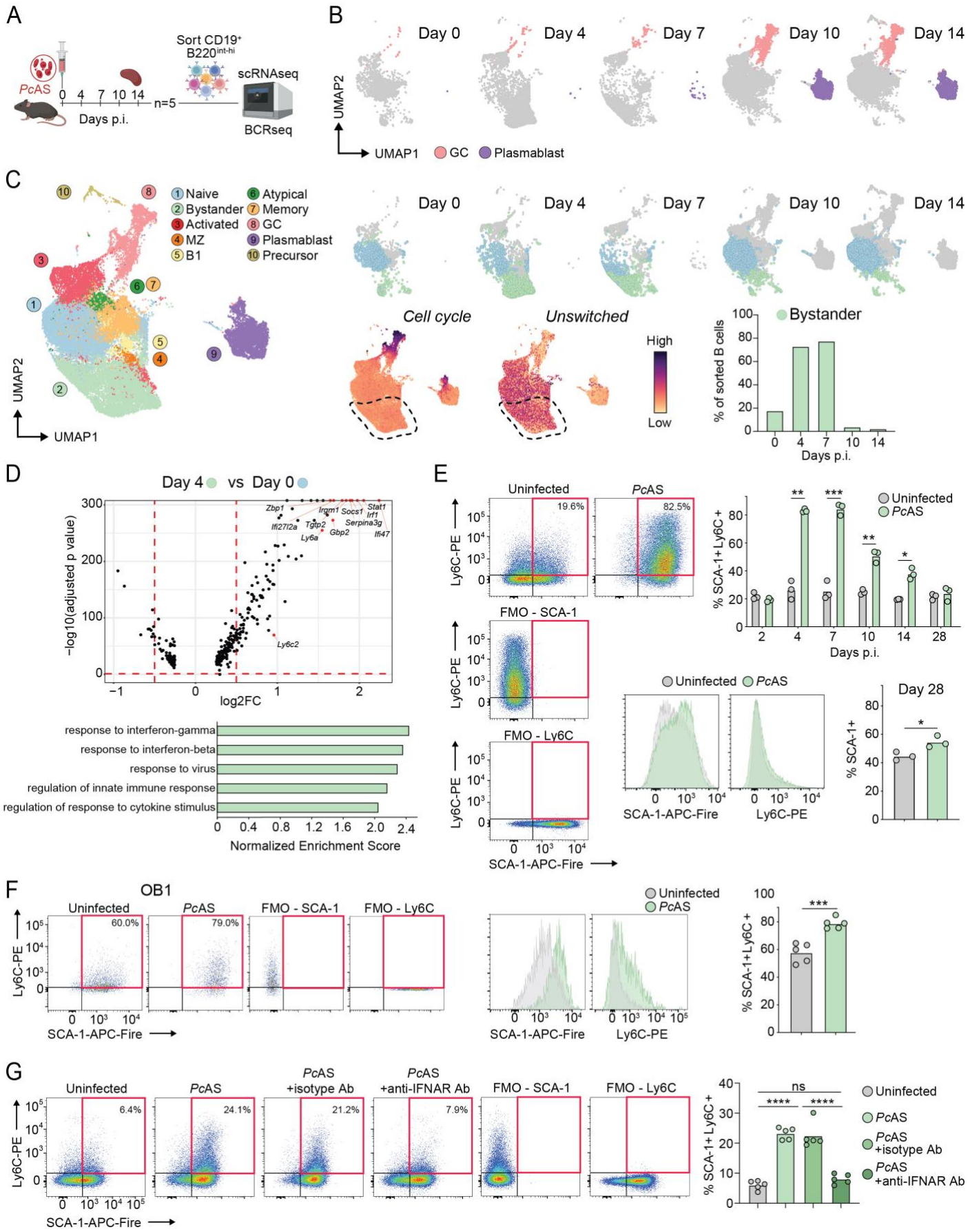

Figure 1: **Antigen-specific B cell differentiation temporally overlaps with bystander B cell activation in experimental malaria.**

(A) Experimental plan to study B cell differentiation in *Pc*AS infected mice sorting $CD19^{+}$ $B220^{int\text{-}hi}$ splenic B cells at various timepoints p.i. to perform droplet-based, paired single cell RNA and BCR sequencing. (B) High dimensional clustering UMAP split by days p.i, highlighting in pink, GC B cells and in purple, plasmablasts. (C) High dimensional clustering UMAP showing combined B cell data and split by timepoints with the two follicular subsets (naive in blue and bystander population highlighted in green) and remaining B cells (grey). Also shown are cell cycle signature and unswitched signature feature plots where dashed lines highlight the bystander population, plus graph showing proportion of bystander population over the course of infection. (D) Volcano plot highlighting in red the top differentially upregulated genes expressed in the day 4 bystander follicular cluster compared to day 0 naive follicular cluster. Gene set enrichment analysis (GSEA) highlights the top five significantly enriched biological processes gene ontology (GO) terms. (E) Representative density plots of SCA-1 and Ly6C expression ("bystander markers") in IgD^{+} B cells at day 4 post-*Pc*AS infection and bar graph of the frequency of SCA-1^{+} $Ly6C^{+}$ cells amongst IgD^{+} B cells over the course of a *Pc*AS infection. Also shown are representative FACS histograms of SCA-1 and Ly6C expression and bar graph of proportion of SCA-1^{+} in day 28 post-infected IgD^{+} B cells. (F) Representative density dot plots, histograms and bar graph showing proportion of SCA-1 and Ly6C expression on $CD86^{lo}$ OB1 adoptively transferred B cells, 4 days post-*Pc*AS infection. (G) Representative density plots of SCA1 and Ly6C expression at day 4 post-*Pc*AS infection in the presence of continual anti-IFNAR blockade or isotype control antibody. Bar plots in panels E-G represented as mean value and panels E-F analysed using Welch's *t*-test and panel G by one-way ANOVA with Tukey's multiple comparisons test. All experiments are representative of two independent experiments with n = 3-5 biological replicates per group. *p <0.05, **p <0.01, ***p <0.001, ****p <0.0001.

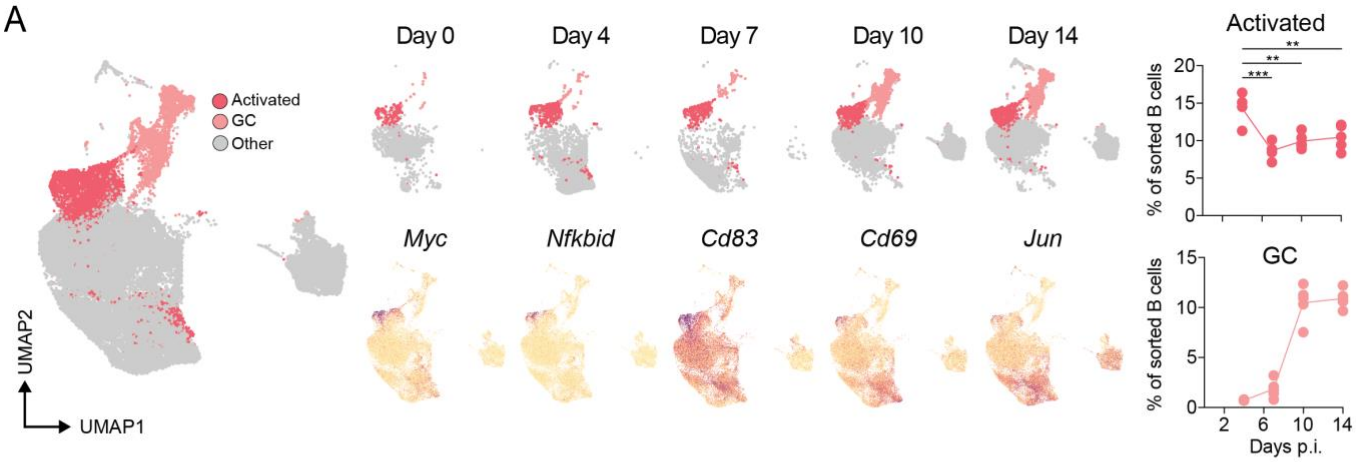
A
Activated
GC
Other
UMAP2
UMAP1
Day 0
Day 4
Day 7
Day 10
Day 14
Myc
Nfkbid
Cd83
Cd69
Jun
Activated
% of sorted B cells
GC
Days p.i.

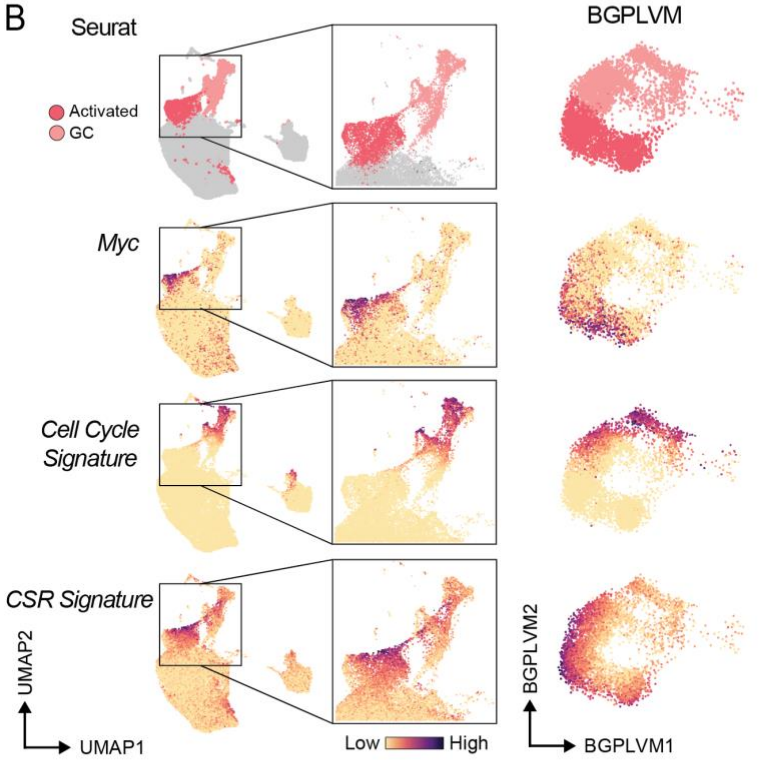
B
Seurat
Activated
GC
Myc
Cell Cycle Signature
CSR Signature
UMAP2
UMAP1
Low
High
BGPLVM
BGPLVM2
BGPLVM1

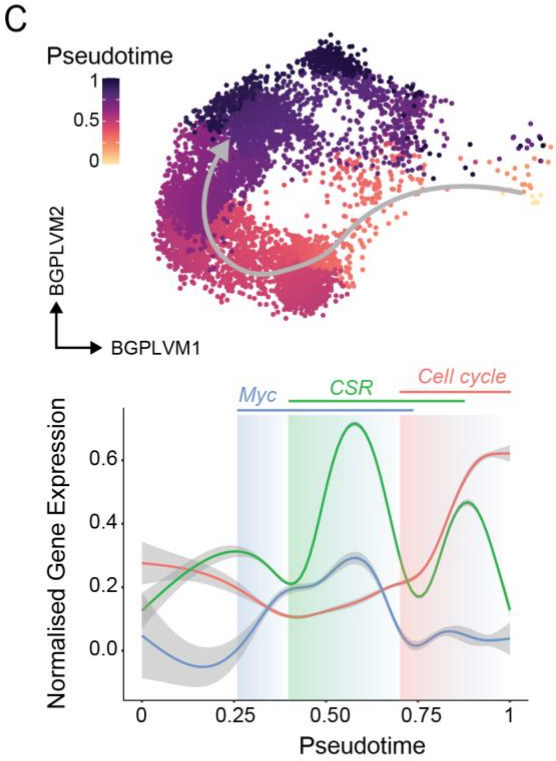
C
Pseudotime
BGPLVM2
BGPLVM1
Myc
CSR
Cell cycle
Normalised Gene Expression
Pseudotime

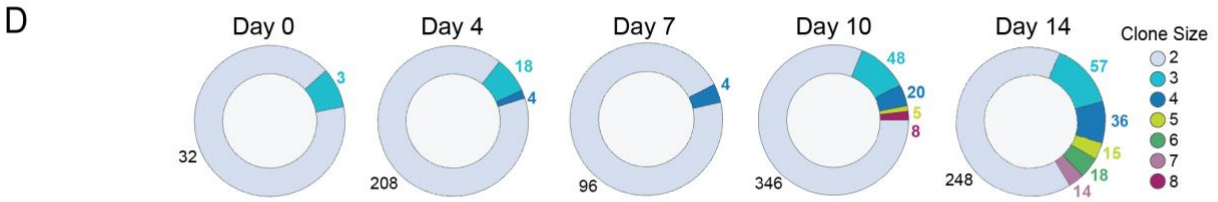
D
Day 0
Day 4
Day 7
Day 10
Day 14
Clone Size

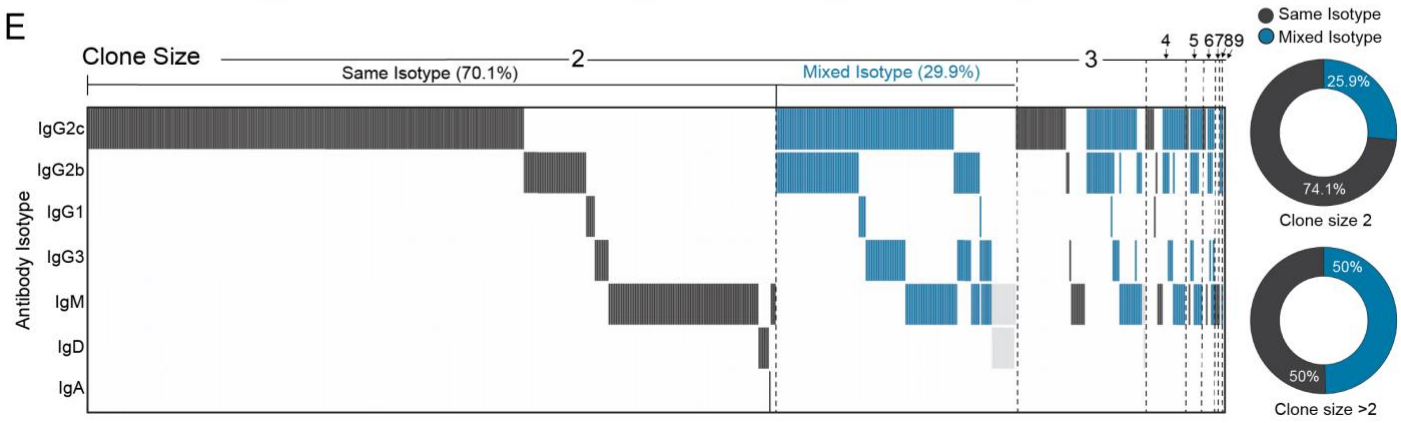
E
Clone Size
Same Isotype (70.1%)
Mixed Isotype (29.9%)
Same Isotype
Mixed Isotype
Antibody Isotype
IgG2c
IgG2b
IgG1
IgG3
IgM
IgD
IgA
Clone size 2
Clone size >2

Figure 2: CSR occurs early during infection, overlapping with *Myc* upregulation and clonal expansion.

(A) Annotated B cell UMAP of activated (indicated by activation marker gene expression: *Myc, Nfkbid, Cd83, Cd69* and *Jun*) and GC B cells after high dimensional reduction. Clustering is additionally split by each timepoint with quantitation of replicate mice across time for activated and GC B cells. (B) Feature plots of *Myc* expression, CSR gene and signature and cell cycle signature across two different embeddings: Seurat and Bayesian Gaussian Process Latent Variable Model (BGPLVM). (C) Pseudotime trajectory analysis of BGPLVM object using GPFates, including *Myc*, CSR signature and cell cycle signature normalised expression along pseudotime. (D) Donut plots of total clone sizes over the course of infection showing frequency of clones for each clone size (coloured) per timepoint. (E) Plot showing the isotype fates of clones at Day 10 and 14 p.i. for each clone size, pooled from two independent experiments. Each column defines a single clone, split by same isotype (dark grey) or mixed isotype (blue). Donut plot shows the quantification of same and mixed isotypes for clones of size 2 or greater than 2. Lines connect the mean value in panel A at each timepoint and analysed by one-way ANOVA with Tukey's multiple comparisons test. $^{**}p < 0.01$, $^{***}p < 0.001$.

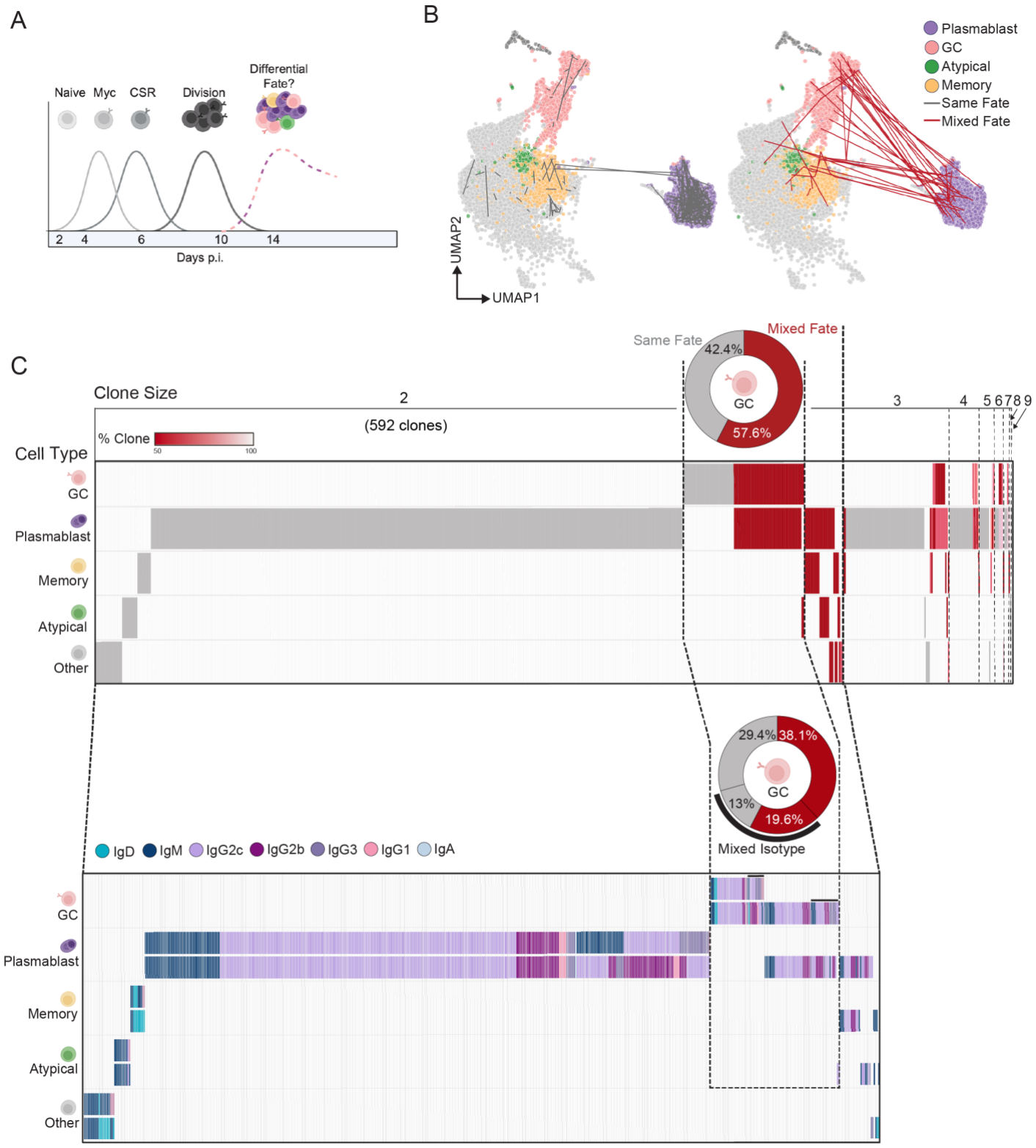

Figure 3: GC B cell clones exhibit phenotypic diversity and isotype variegation.

(A) Schematic showing the emergence of different B cell dynamics during the course of malaria infection, next determining the differential fate of naive B cells. (B) Annotated B cell UMAP after performing V(D)J analysis of day 10 and 14 p.i. combined. Cells sharing same fate (black lines) or mixed fates (red lines) for indicated cell fates: plasmablast, GC, memory, atypical and remaining B cell fates (grey) are connected by lines. (C) Plots showing the clonal fates ordered by clonal size of plasmablast, GC, memory, atypical and other at Day 10 and 14 p.i. (combined experiment 1 and 2). Each row represents cell fate, and each column represents the % cells per clone. Clones are split

by same fate (grey) and mixed fate (red). The donut chart shows the quantification of same (grey) and mixed fates (red) in GC containing clones of size 2. Clones of size 2 (of which there were 592 clones in total) were further analysed for their isotype in each cell, with donut chart showing quantitation of same and mixed isotypes (denoted with thick black line) for each clone with same (grey) and mixed fate (red) outcomes.

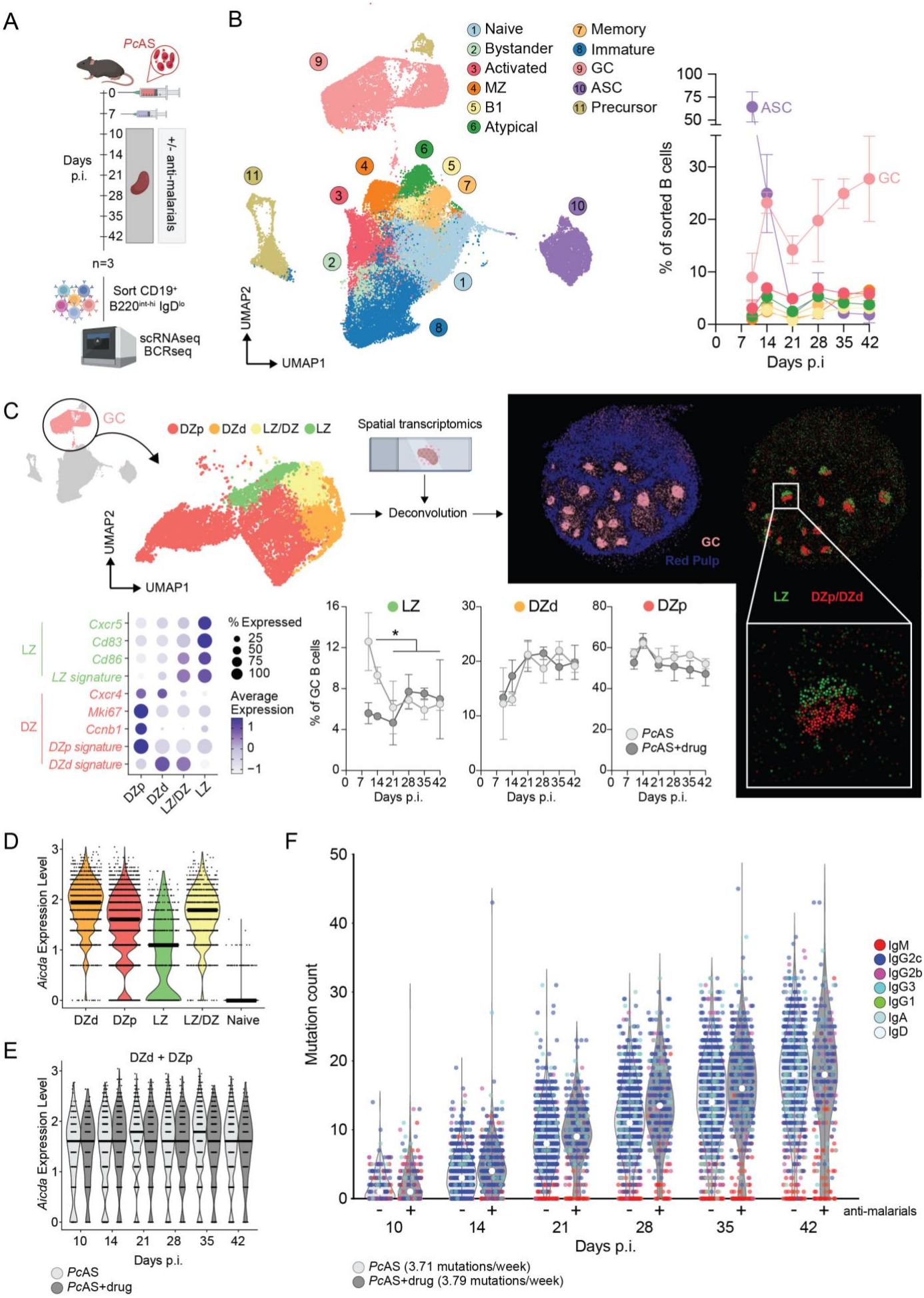
A
PcAS
Days p.i.
0
7
10
14
21
28
35
42
+/- anti-malarials
n=3
Sort CD19+ B220int-hi IgDlo
scRNAseq BCRseq
B
1 Naive
2 Bystander
3 Activated
4 MZ
5 B1
6 Atypical
7 Memory
8 Immature
9 GC
10 ASC
11 Precursor
UMAP2
UMAP1
ASC
GC
% of sorted B cells
Days p.i
C
GC
DZp DZd LZ/DZ LZ
Spatial transcriptomics
Deconvolution
GC
Red Pulp
LZ
DZp/DZd
Cxcr5
Cd83
Cd86
LZ signature
Cxcr4
Mki67
Ccnb1
DZp signature
DZd signature
% Expressed
25
50
75
100
Average Expression
% of GC B cells
Days p.i.
PcAS
PcAS+drug
D
Aicda Expression Level
DZd
DZp
LZ
LZ/DZ
Naive
E
DZd + DZp
Days p.i.
F
Mutation count
IgM
IgG2c
IgG2b
IgG3
IgG1
IgA
IgD
anti-malarials
Days p.i.
PcAS (3.71 mutations/week)
PcAS+drug (3.79 mutations/week)

Figure 4: GC B cells maintain diversity and constant SHM after anti-malarial treatment.

(A) Experimental plan to study B cell differentiation in *Pc*AS-infected mice, with or without anti-malarial drug treatment, sorting $CD19^{+}$ $B220^{int\text{-}hi}$ IgD^{lo} splenic B cells at various timepoints p.i. to perform droplet-based, paired single cell RNA and BCR sequencing. (B) Annotated combined UMAP of all mice, treatments and timepoints after high-dimensional reduction and clustering (left), with quantitation (right) of the proportion of selected, annotated B cells over the course of *Pc*AS infection (no drug treatment). (C) Sub-clustering of the GC cluster identifies distinct DZp, DZd, LZ/DZ and LZ GC B cell clusters as indicated in the dot plot of canonical markers and gene signatures of known GC B cell subsets. Also shown is quantitation of different GC B cell populations over time. RCTD spatial deconvolution of GC B cell populations on a day 30, *Plasmodium* infected spleen using *Slide-seqV2* spatial transcriptomics (right). (D) Median *Aicda* gene expression in GC B cell subsets and naive B cells as negative control. (E) Median *Aicda* expression shown overtime, with or without anti-malarial treatment in DZd and DZp GC B cells. (F) Somatic hypermutation analysis of GC B cell BCRs and isotype usage overtime, split by treatment, showing mutation rates for both treatments. Median number of mutations for each treatment and timepoint indicated in white. Data in B-C are shown as mean ± S.D. and analysed by one-way ANOVA with Tukey's multiple comparisons test of $n = 3$ biological replicates. $^{*}p < 0.05$.

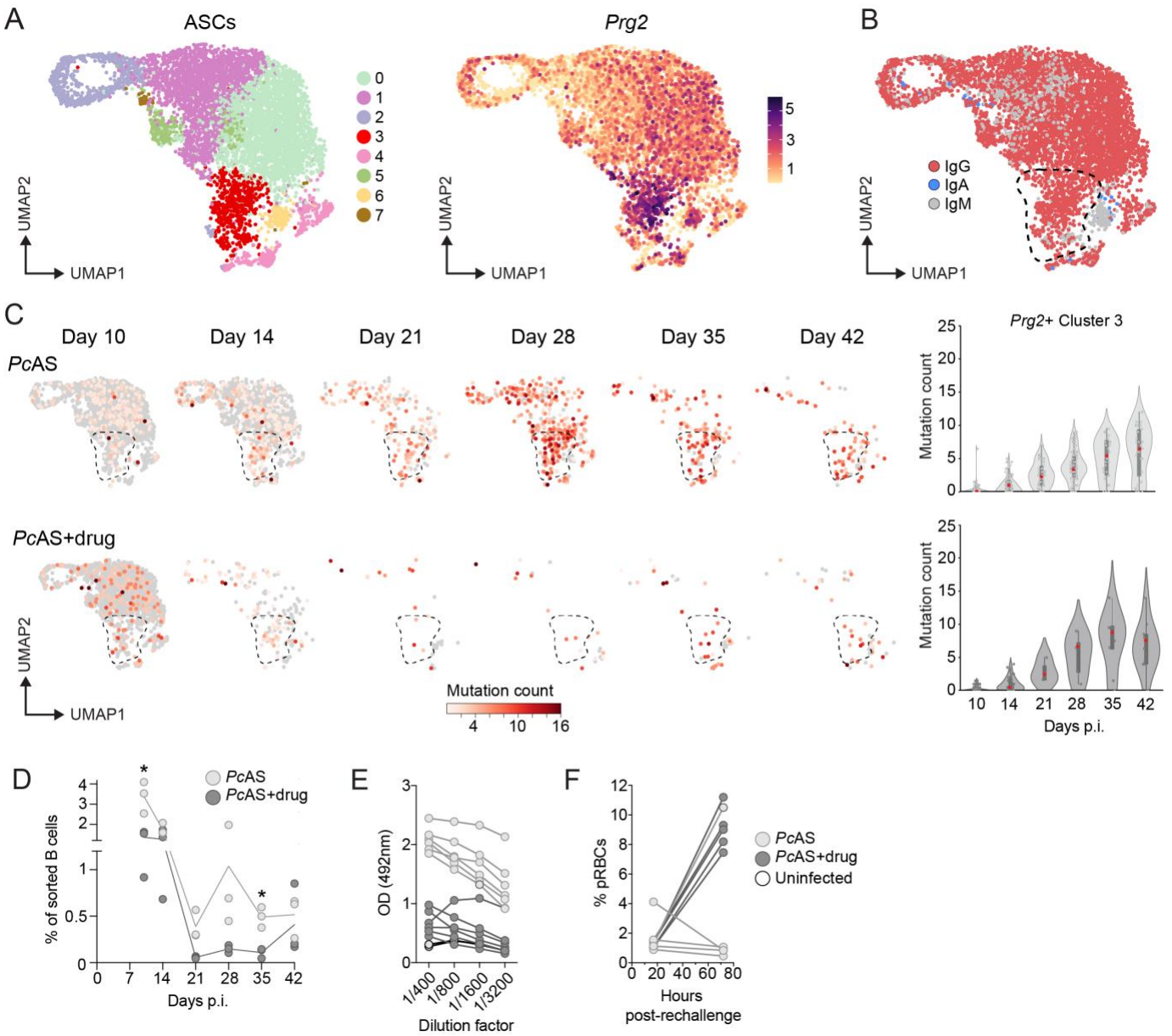

Figure 5: Anti-malarial treatment impairs GC output during experimental malaria.

(A) UMAP of sub-clustered ASCs identifies a cluster highlighted in red consisting of *Prg2*^{hi} splenic plasma cells. (B) UMAP of isotype classification with *Prg2*^{hi} cluster indicated. (C) Mutation counts in the BCR of sub-clustered ASCs, plotted with or without anti-malarial drug treatment and split overtime, *Prg2*^{hi} area indicated by enclosed dashed line and quantified in violin plots (right). Median number of mutations in violin plots highlighted in red. (D) Proportions of *Prg2*^{hi}, cluster 3 plasma cells over the course of infection with or without anti-malarials. (E) ELISA measuring *Plasmodium*-specific IgG levels in the sera of mice at day 60 p.i. with or without anti-malarials. (F) Mice treated with or without anti-malarials during a primary *Pc*AS infection were rechallenged and parasitemia in the blood measured 17 and 72 hours post-rechallenge. Lines in panel D connects the mean values at each timepoint and statistical test performed are Welch's *t*-test. *$p < 0.05$.

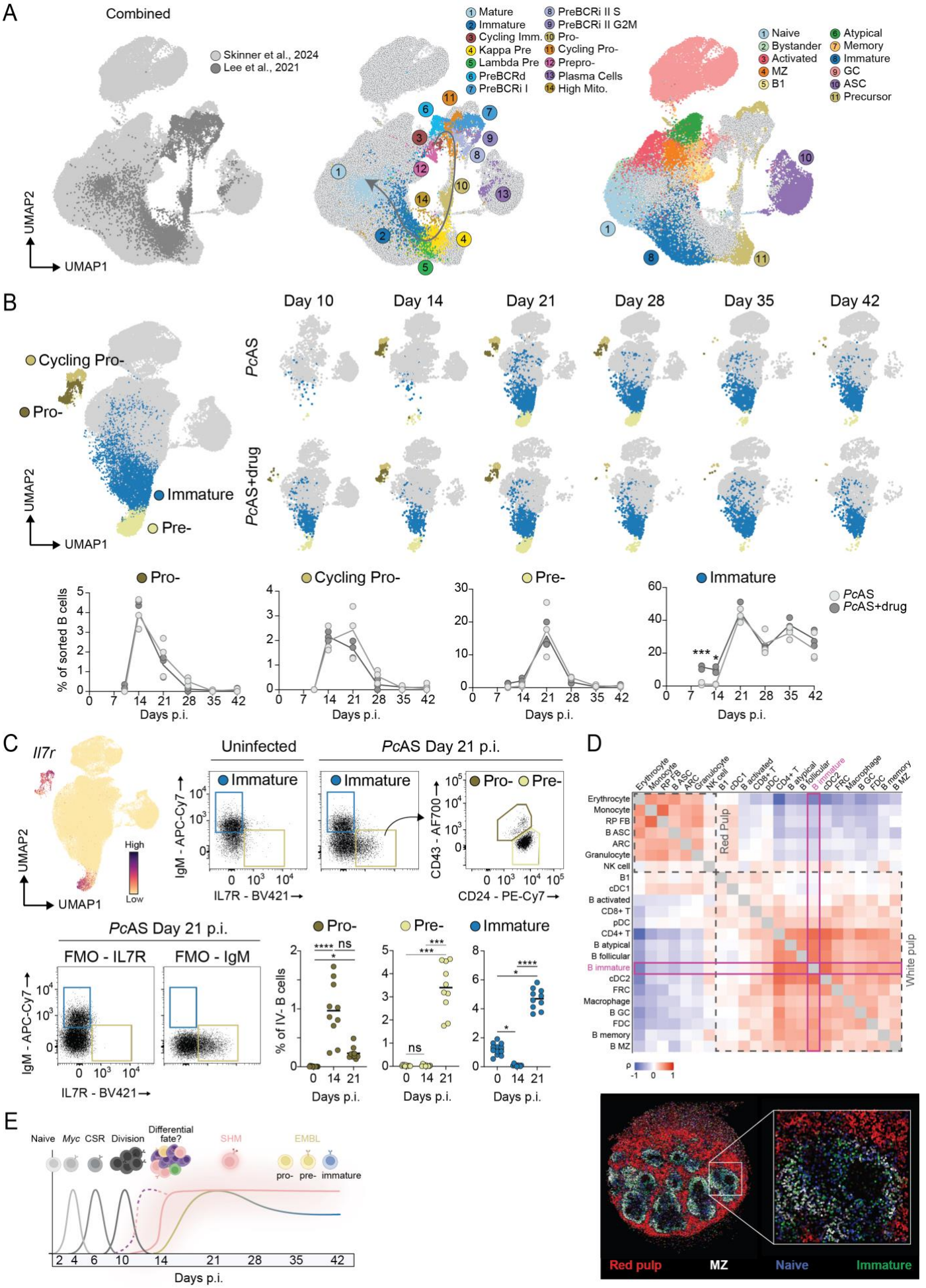
A
Combined
Skinner et al., 2024
Lee et al., 2021
UMAP2
UMAP1
1 Mature
2 Immature
3 Cycling Imm.
4 Kappa Pre
5 Lambda Pre
6 PreBCRd
7 PreBCRi I
8 PreBCRi II S
9 PreBCRi II G2M
10 Pro-
11 Cycling Pro-
12 Prepro-
13 Plasma Cells
14 High Mito.
1 Naive
2 Bystander
3 Activated
4 MZ
5 B1
6 Atypical
7 Memory
8 Immature
9 GC
10 ASC
11 Precursor
B
Day 10
Day 14
Day 21
Day 28
Day 35
Day 42
Cycling Pro-
Pro-
Immature
Pre-
PcAS
PcAS+drug
Pro-
Cycling Pro-
Pre-
Immature
% of sorted B cells
Days p.i.
PcAS
PcAS+drug
C
Il7r
High
Low
Uninfected
PcAS Day 21 p.i.
Immature
IgM - APC-Cy7
IL7R - BV421
CD43 - AF700
CD24 - PE-Cy7
Pro-
Pre-
FMO - IL7R
FMO - IgM
% of IV- B cells
ns
D
Erythrocyte
Monocyte
RP FB
B ASC
ARC
Granulocyte
NK cell
B1
cDC1
B activated
CD8+ T
pDC
CD4+ T
B atypical
B follicular
B immature
cDC2
FRC
Macrophage
B GC
FDC
B memory
B MZ
Red Pulp
White pulp
ρ
E
Naive
Myc
CSR
Division
Differential fate?
SHM
EMBL
pro-
pre-
immature
Days p.i.
Red pulp
MZ
Naive
Immature

Figure 6: B cell lymphopoiesis relocates to the spleen during experimental malaria.

(A) scVI integration of our day 10-42 B cell dataset with publicly available scRNAseq bone marrow data combined and split by each dataset, with arrow indicating inferred trajectory of Lee et al., 2021 dataset. (B) Annotated B cell scVI integrated UMAP (experiment 1 and experiment 2) of specific precursor B cell subsets during extramedullary B lymphopoiesis: pro-, cycling pro-, pre- and immature B cells split overtime, with or without anti-malarial drug treatment and quantified per replicate mouse. (C) *Il7r* gene expression highlighted on proB and preB cells. IL7R surface marker used to identify precursor B cells shown by representative flow cytometry panel of B cells gated on CD45.2^{-} (intravenous label negative, IV^{-}), CD19^{+} B220^{+} CD138^{-} CD38^{+} Fas^{-} IgD^{-} CD93^{+} for immature B cells (IgM^{+} IL7R^{-}), pro-B cells (IgM^{-} IL7R^{+}, CD43^{hi} CD24^{int}) and pre-B cells (IgM^{-} IL7R^{+}, CD43^{int} CD24^{hi}) in uninfected mice and at day 21 post-*Pc*AS infection, with quantitation of splenic precursor B cells at 0, 14 and 21 days p.i. (D) RCTD spatial deconvolution of immature B cell populations from *Plasmodium* infected spleen at day 30 p.i. using *Slide-seqV2* spatial transcriptomics, showing spearman's correlation analysis of cell co-localisations from a scRNAseq reference with location of selected populations including immature B cells (green) plotted on the array. (E) Schematic of different B cell dynamics including extramedullary B lymphopoiesis (EMBL) in our *Plasmodium* infection system. Lines in panel B connect the mean values at each timepoint and analysed by Welch's *t*-test and panel C by one-way ANOVA with multiple comparisons test of n = 10-20 pooled from 2 independent experiments. Data in panel C are the mean value. *$p < 0.05$, *** $p < 0.001$, **** $p < 0.0001$. ns, not significant.

Extended Data Figures

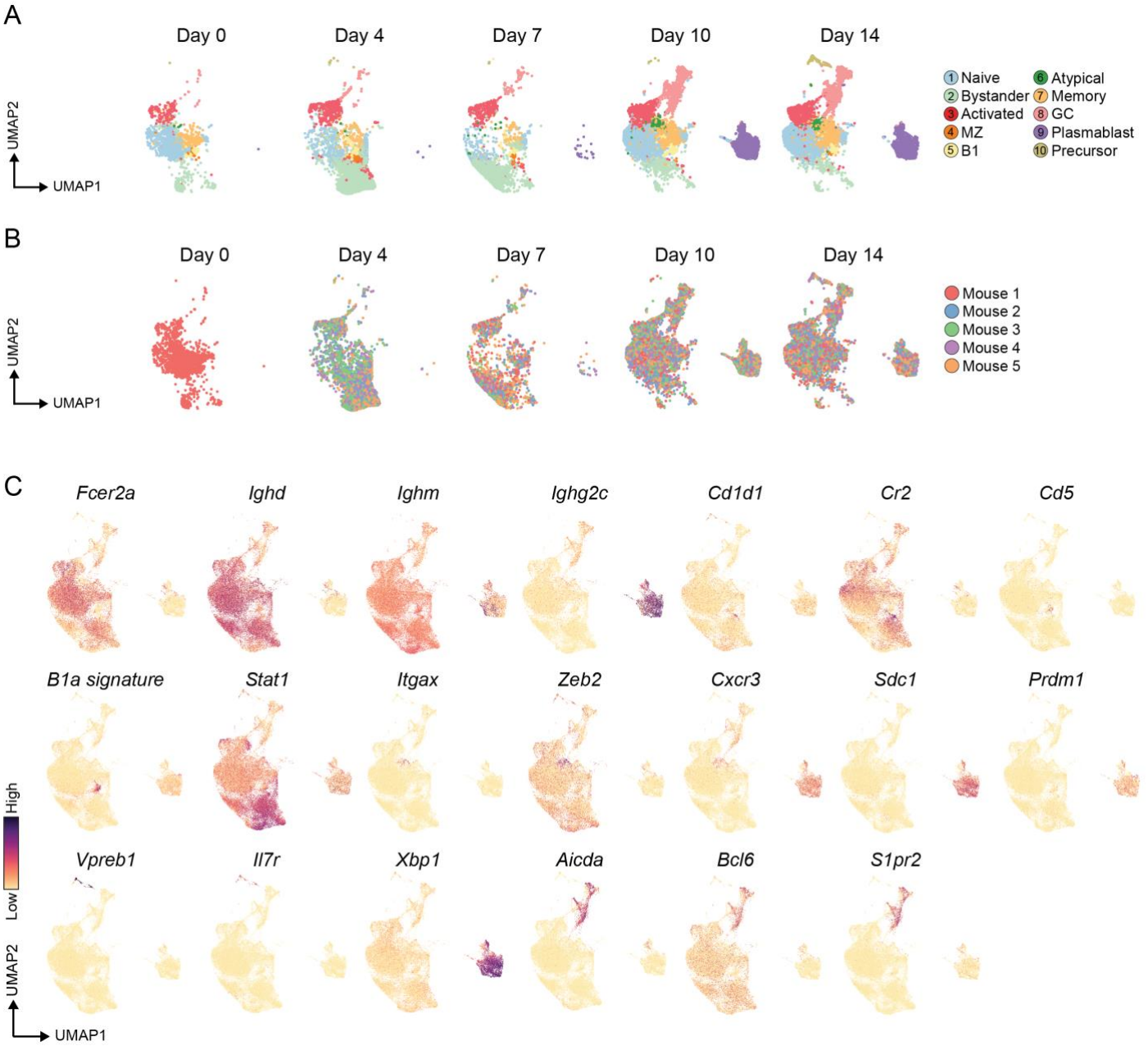

Extended Data Figure 1: Cluster annotation of B cell scRNAseq data (Experiment 1).

(A) Annotation of B cell subsets after high dimensional reduction and clustering analysis, split by timepoints and (B) grouped by individual mice. (C) Expression of canonical markers for each cluster type: naive follicular B cells (*Fcer2a*, unswitched: *Ighd*$^{+}$*, Ighm*$^{+}$*, Ighg2c*$^{-}$), MZ cells (*Cd1d1, Cr2*), B1 cells (*Cd5, B1a signature*), bystanders (*Stat1*), precursor B cells (*Vpreb1, Il7r*), atypicals (*Itgax, Zeb2, Cxcr3*), plasmablasts (*Sdc1, Prdm1, Xbp1*, switched: *Ighd*$^{-}$*, Ighg2c*$^{+}$) and GC B cells (*Aicda, Bcl6, S1pr2,* switched: *Ighd*$^{-}$*, Ighg2c*$^{+}$).

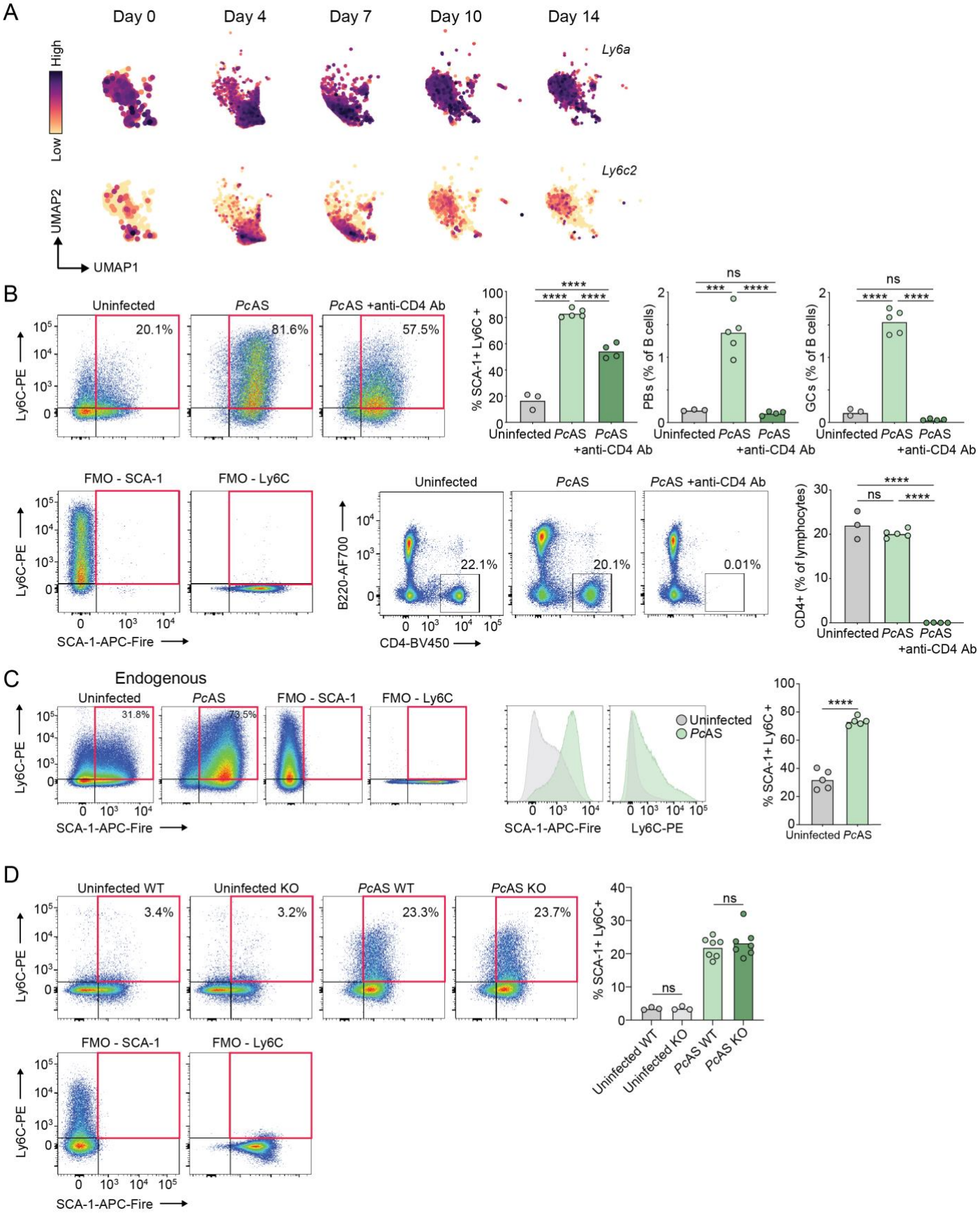

Extended Data Figure 2: Bystander B cell activation occurs in the absence of CD4⁺ T cells, and is independent of MyD88-signalling.

(A) Expression of *Ly6a* (Sca-1) and *Ly6c2* on naive follicular and bystander B cells over the course of *Plasmodium* infection. (B) Representative density dot plots and bar graphs of CD4 expression on

lymphocytes 7 days post-*Pc*AS infection, and SCA-1 and Ly6C expression on IgD^+ B cells, and frequency of plasmablast and GC B cells relative to all B cells 7 days post *Pc*AS infection, with or without CD4 T cell depletion. (C) Representative density dot plots, histograms and bar graph showing proportion of SCA-1 and Ly6C expression on $CD86^{lo}$, IgD^+ endogenous host derived B cells from the OB1 adoptive transfer experiments, 4 days post-*Pc*AS infection. (D) Representative density dot plots, and bar graph showing proportion of SCA-1 and Ly6C expression on IgD^+ MyD88flox/flox B cells with ($CD23^{cre+/-}$ KO) or without ($CD23^{cre-/-}$ WT) MyD88 KO, 7 days post-*Pc*AS infection. Data in panels B-D are represented as the mean value. Data in panel B and D analysed using one-way ANOVA with Tukey's multiple comparisons test and data in panel C analysed using Welch's *t*-test. All data are representative of two independent experiments of (B & C) n = 3-5 and (D) n = 3-7 biological replicates per group. ***$p < 0.001$, ****$p < 0.0001$. ns, not significant.

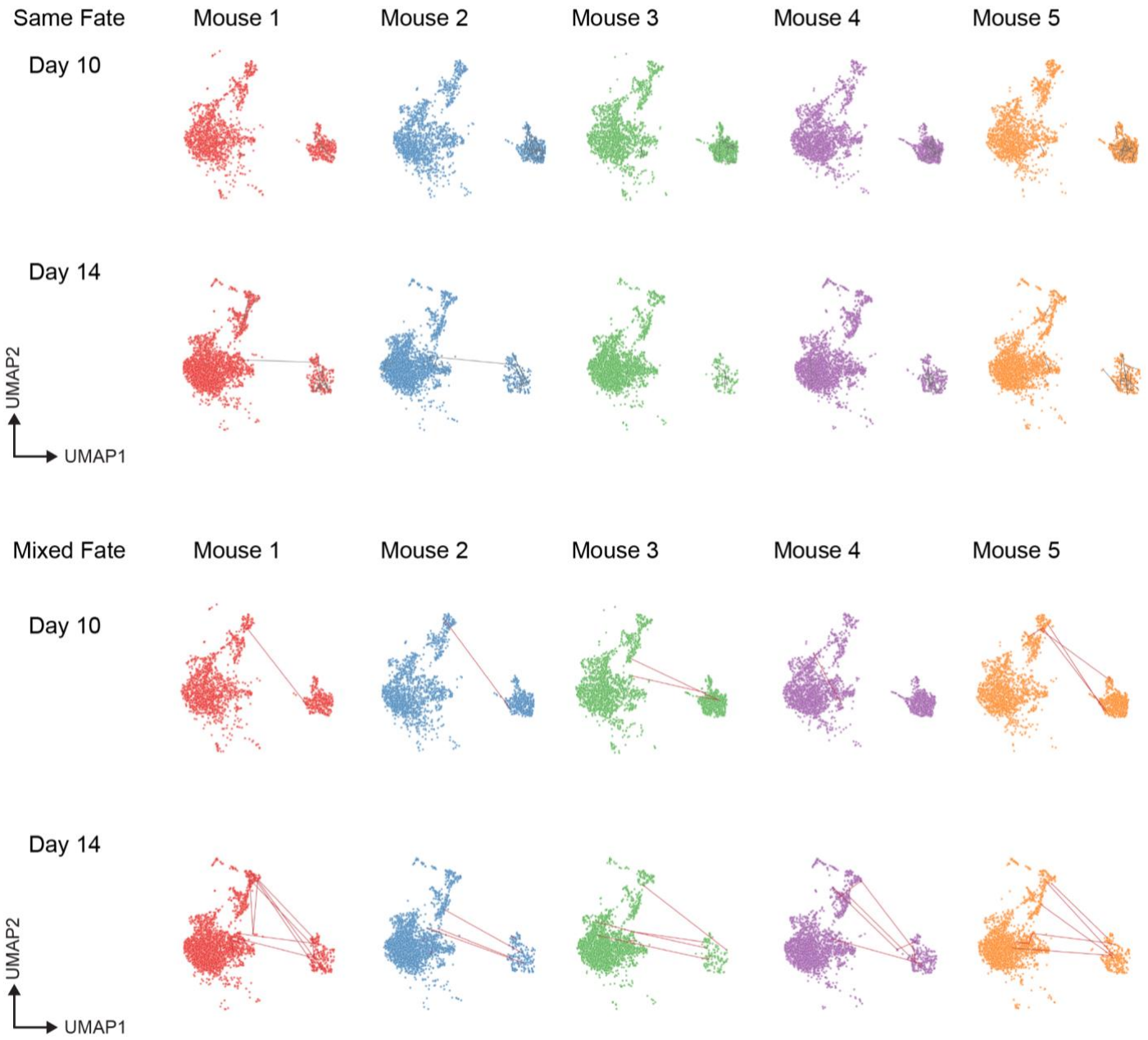

Extended Data Figure 3: Examining "same" vs "different" clonal fates (Experiment 1).

UMAP of same and mixed fate clones in day 10-14 post-*Plasmodium*-infected B cells, split by timepoint, individual mice and by same and mixed fates.

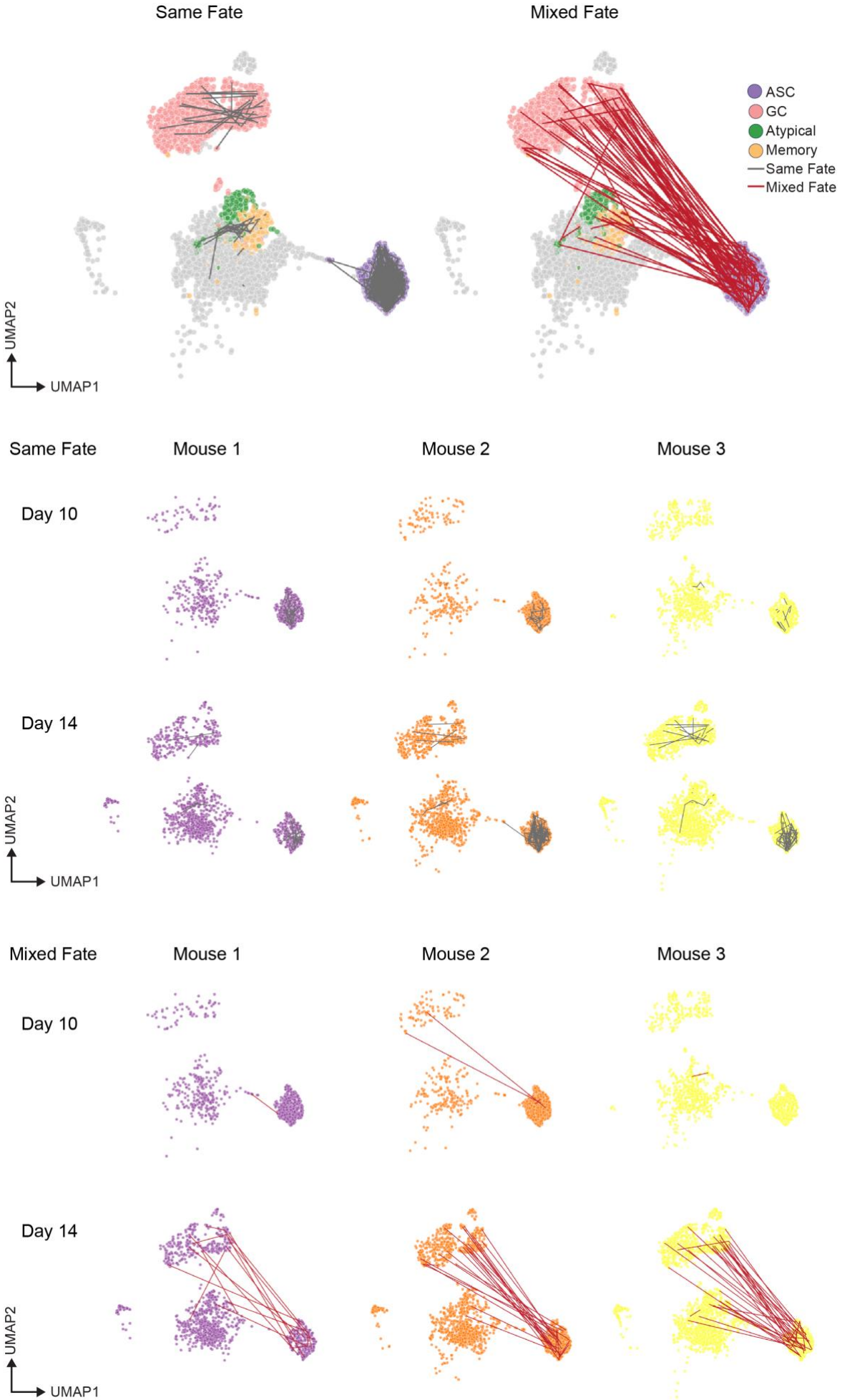
Same Fate
Mixed Fate
ASC
GC
Atypical
Memory
Same Fate
Mixed Fate
UMAP2
UMAP1
Same Fate
Mouse 1
Mouse 2
Mouse 3
Day 10
Day 14
UMAP2
UMAP1
Mixed Fate
Mouse 1
Mouse 2
Mouse 3
Day 10
Day 14
UMAP2
UMAP1

Extended Data Figure 4: Examining “same” vs “different” clonal fates (Experiment 2).

UMAP of same and mixed fate clones in day 10-14 post-*Plasmodium*-infected B cells, split by timepoint, individual mice and by same and mixed fates.

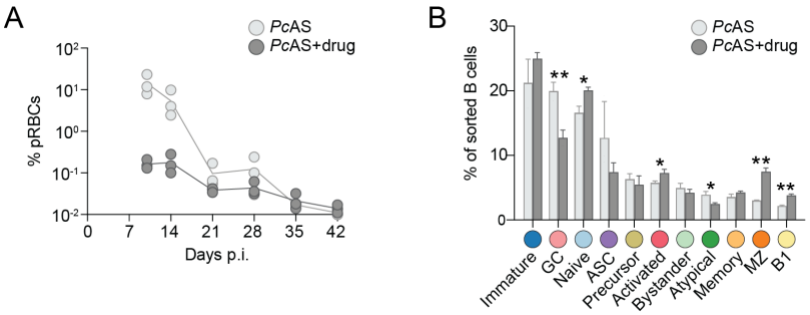

Extended Data Figure 5: Anti-malarial treatment efficacy, and effects on proportions of B cell subsets.

(A) Percentage parasitemia of circulating RBCs at each timepoint post with or without anti-malarials. Lines connect the mean values at each timepoint. (B) For the combined day 10-42 scRNAseq dataset, proportion of each B cell subset under each condition (*Pc*AS or *Pc*AS+drug) for individual mice. Data are the mean ± S.D, statistical test used was Welch's *t*-test. *p <0.05, ** p <0.01.

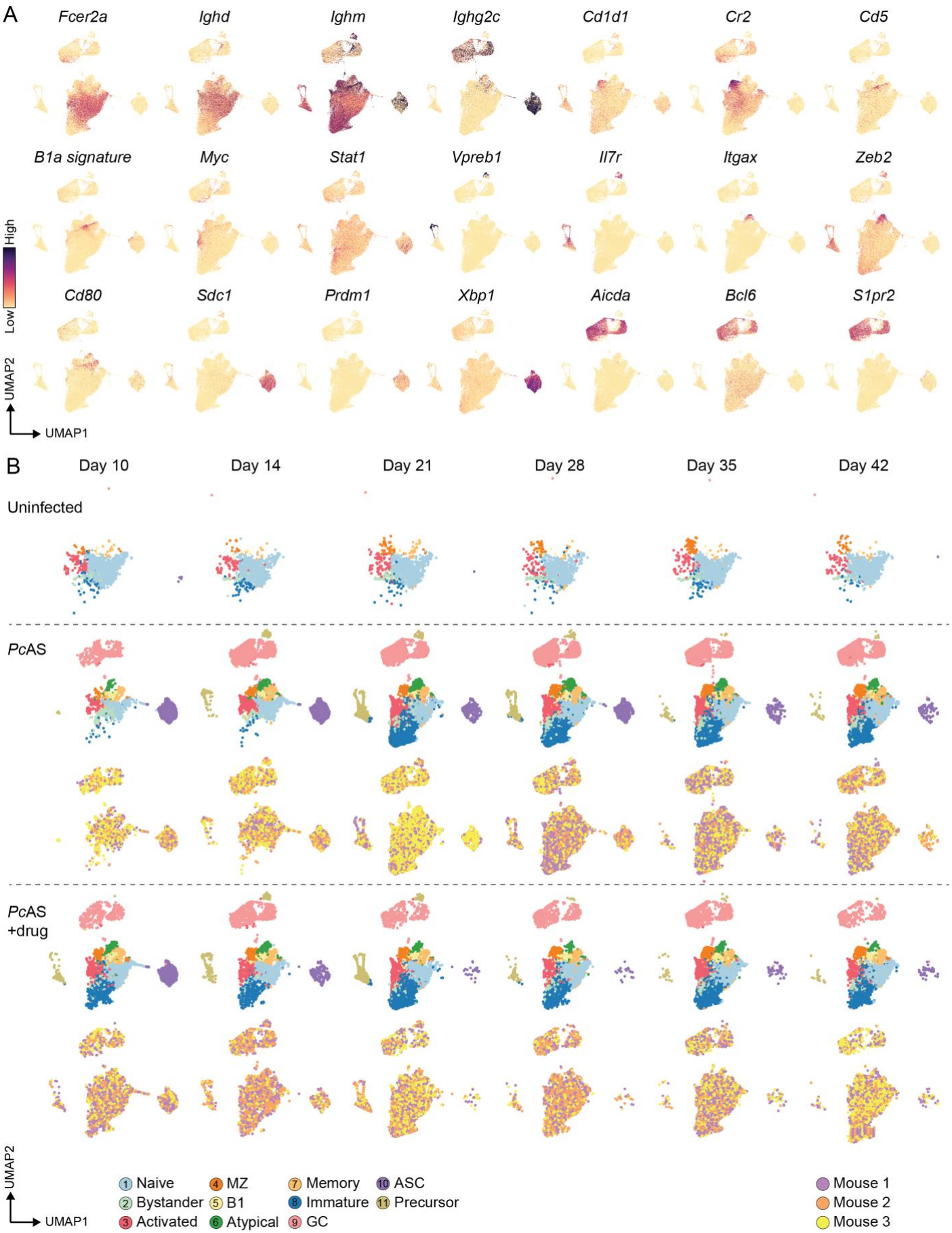

Extended Data Figure 6: Cluster annotation of B cell scRNAseq data (Experiment 2).

(A) Expression of canonical markers for each cluster type: naive follicular B cells (*Fcer2a*, unswitched: *Ighd*$^{+}$*, Ighm*$^{+}$*, Ighg2c*$^{-}$), MZ cells (*Cd1d1, Cr2*), B1 cells (*Cd5, B1a signature*), activated B cells (*Myc*), bystanders (*Stat1*), precursor B cells (*Vpreb1, Il7r*), atypicals (*Itgax, Zeb2*), memory B cells (*Cd80*), plasmablasts (*Sdc1, Prdm1, Xbp1*, switched: *Ighd*$^{-}$*, Ighg2c*$^{+}$) and GC B cells (*Aicda, Bcl6, S1pr2,* switched: *Ighd*$^{-}$*, Ighg2c*$^{+}$). (B) Annotated UMAPs split by timepoint for each condition: uninfected, *Pc*AS or *Pc*AS+drug also grouped by individual mice.

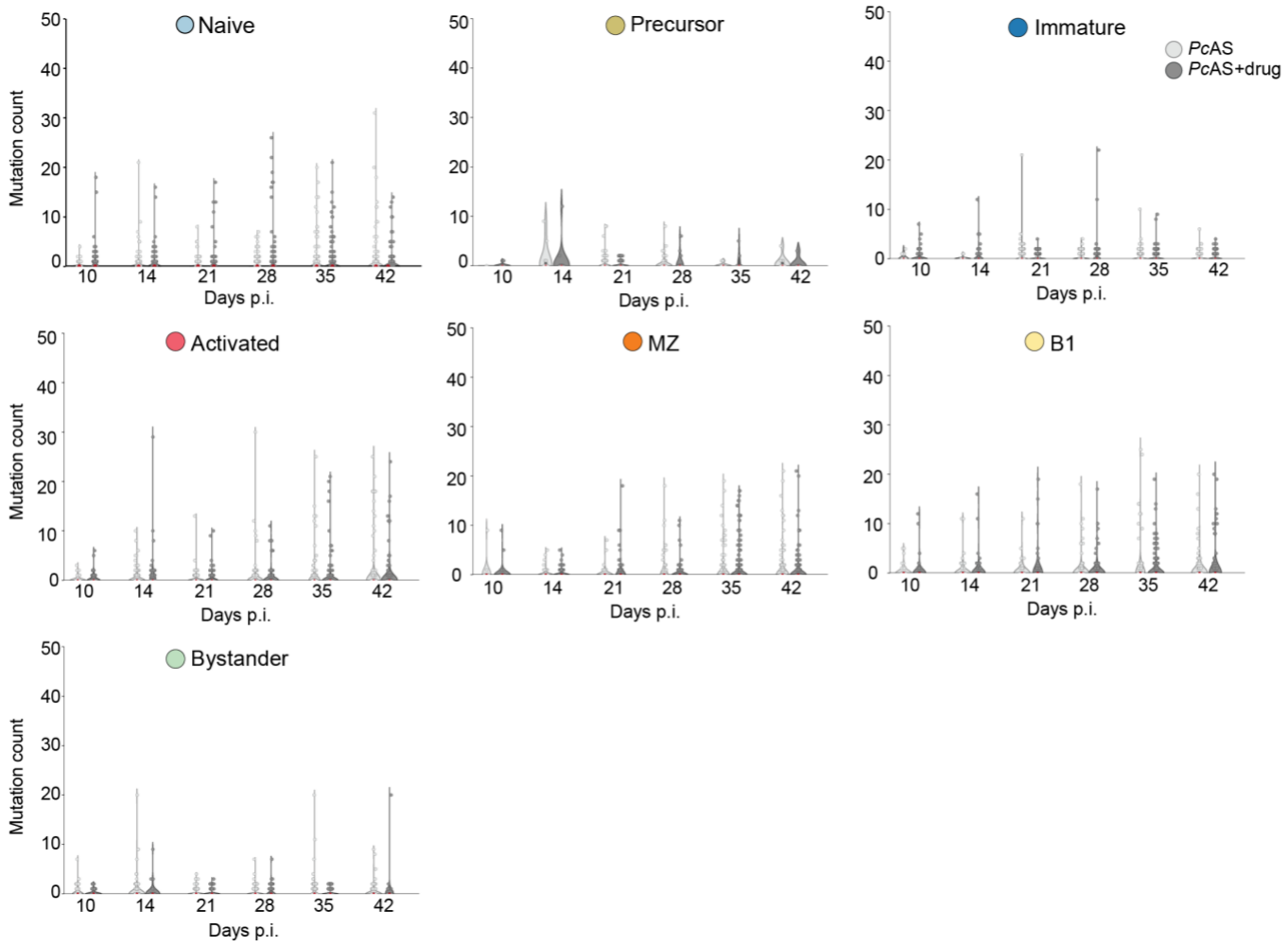

Extended Data Figure 7: BCR mutation counts across B cell populations.

Somatic hypermutation analysis of various B cells (naive, precursor, immature, activated, MZ, B1 and bystander B cells) over the course of *Plasmodium* infection, split by treatment. Median number of mutations highlighted in red.

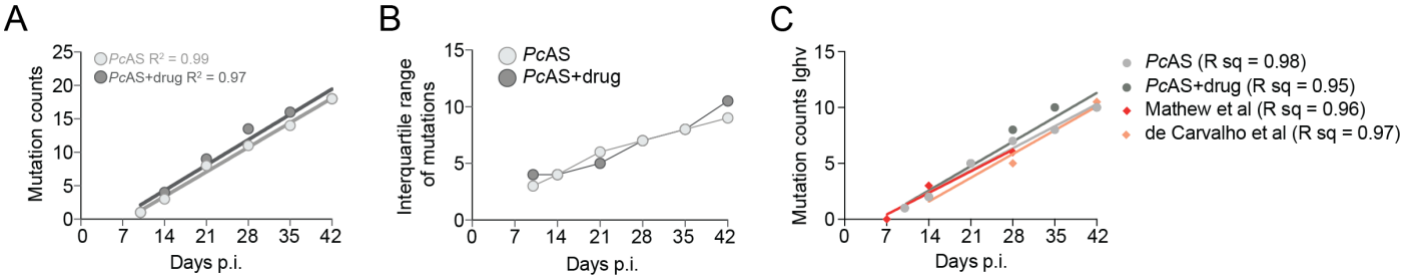

Extended Data Figure 8: GC B cell mutation count and spread increase over time, and are refractory to anti-malarial drug treatment.

(A) For GC B cells the median number of mutations with linear regression for each condition. (B) Interquartile range (IQR) of GC B cell mutations at each timepoint. (C) Median number of mutations in the Ighv region of the BCR for each condition in comparison to clonal data from lymph node GC B cells after influenza infection from Mathew et al. and de Carvalho et al.

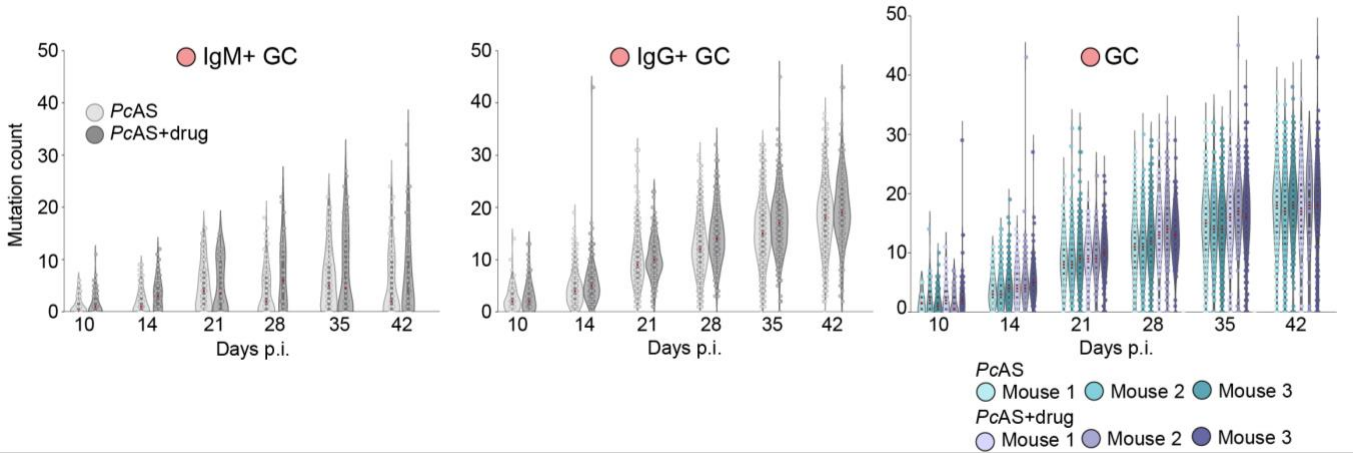

Extended Data Figure 9: BCR mutation counts across GC B cells.

Somatic hypermutation analysis of GC B cells over the course of *Plasmodium* infection, split by treatment, shown as unswitched (IgM^+) and switched (IgG^+) and also shown mutations in all GC B cells split by individual mice. Median number of mutations highlighted in red.

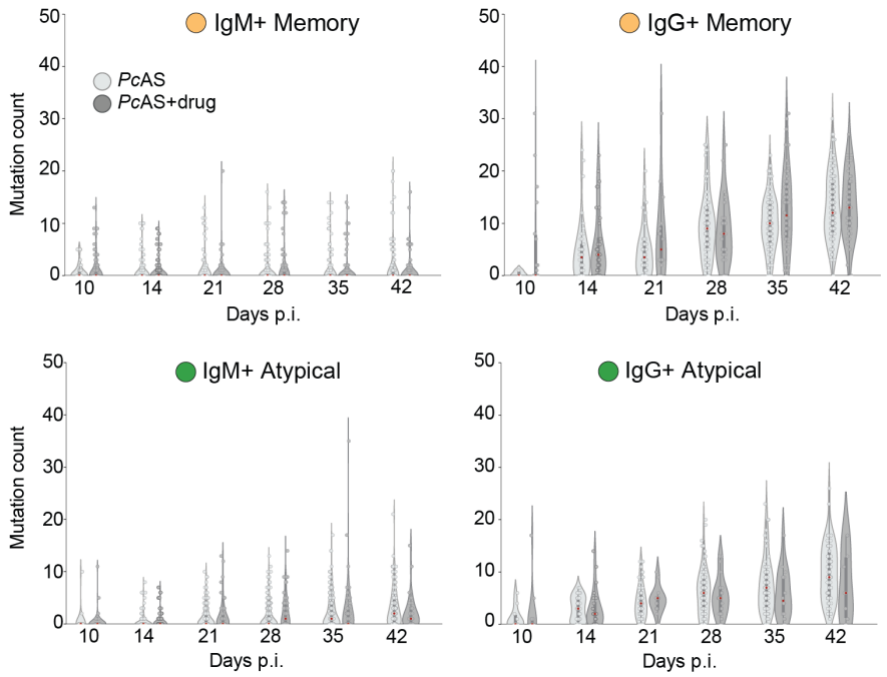

Extended Data Figure 10: BCR mutations across GC-derived B cell populations.

Somatic hypermutation analysis of memory and atypical B cells split by unswitched (IgM^+) and switched (IgG^+) over the course of *Plasmodium* infection, split by treatment. Median number of mutations highlighted in red.

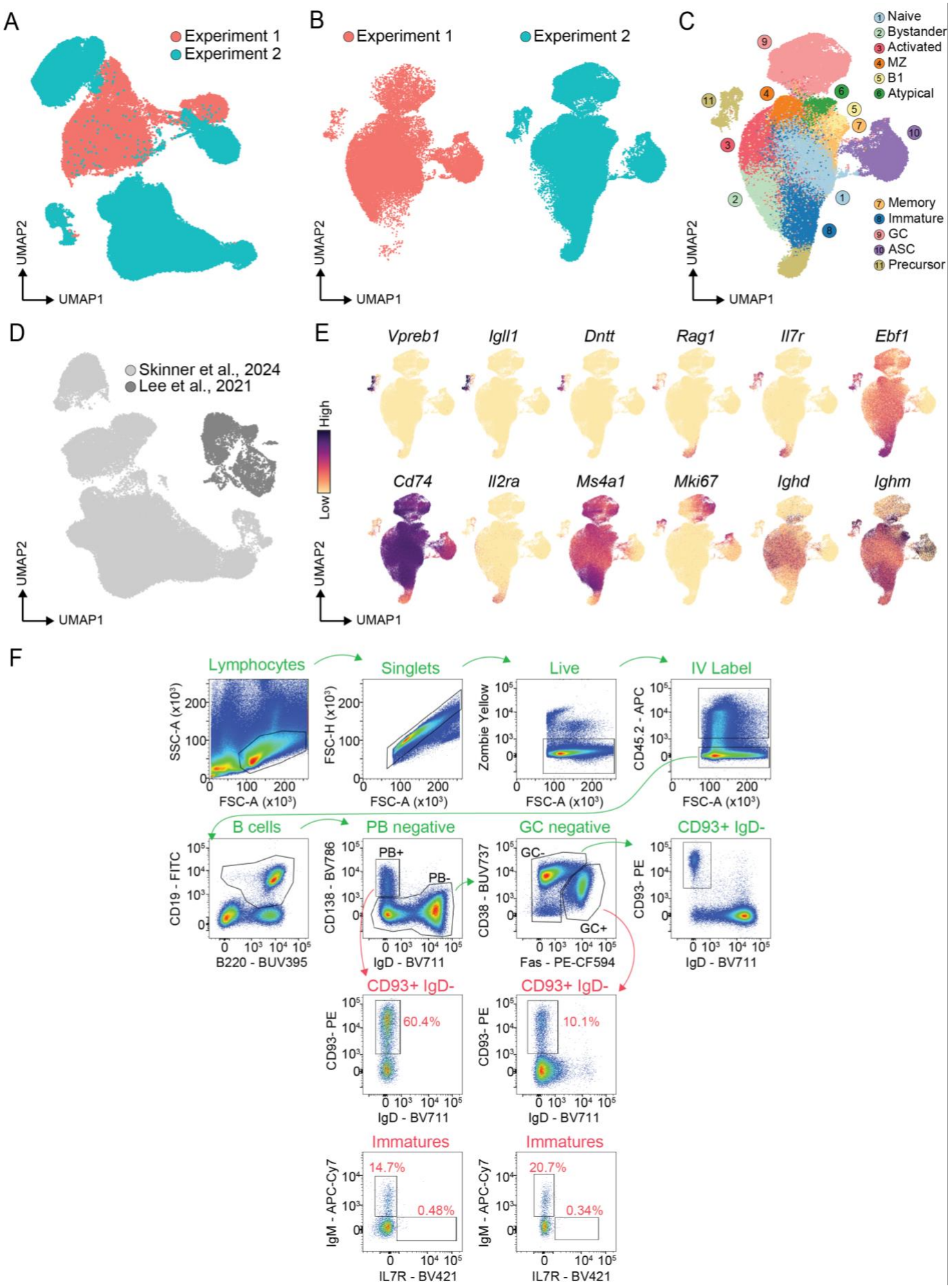

Extended Data Figure 11: Identifying transcriptional and protein markers of extramedullary B lymphopoiesis.

(A) scVI integration of experiment 1 and 2 without batch correction. (B) Integrated scVI UMAP of experiment 1 and 2, using batch correction, split by experiment. (C) Annotated, scVI integrated UMAP of both experimental datasets. (D) scVI integration of our day 10-42 B cell dataset and publicly available bone marrow B cell scRNAseq dataset, without batch correction. (E) Expression of canonical markers of pro-B cells (*Vpreb1, Igll1, Dntt*), cycling pro-B cells (*Mki67*), pre-B cells (*Il2ra*), both pro- and pre-B cells (*Rag1, Il7r, Ebf1, Cd74*^{lo}*, Ighd*$^{-}$) and immature B cells (*Ms4a1, Ighd*$^{-}$*, Ighm*$^{+}$). (F) Gating strategy for investigating splenic precursor B cells after *Plasmodium* infection by gating on live CD45.2^{-} CD19^{+} B220^{+} B cells, CD138^{-} IgD^{+} non-plasmablasts, CD38^{+} Fas^{-} non-GCs and IgD^{-} CD93^{+} to look for immature B cells (IgM^{+} IL7R^{-}) and pre- and pro-B cells (IgM^{-} IL7R^{+}).

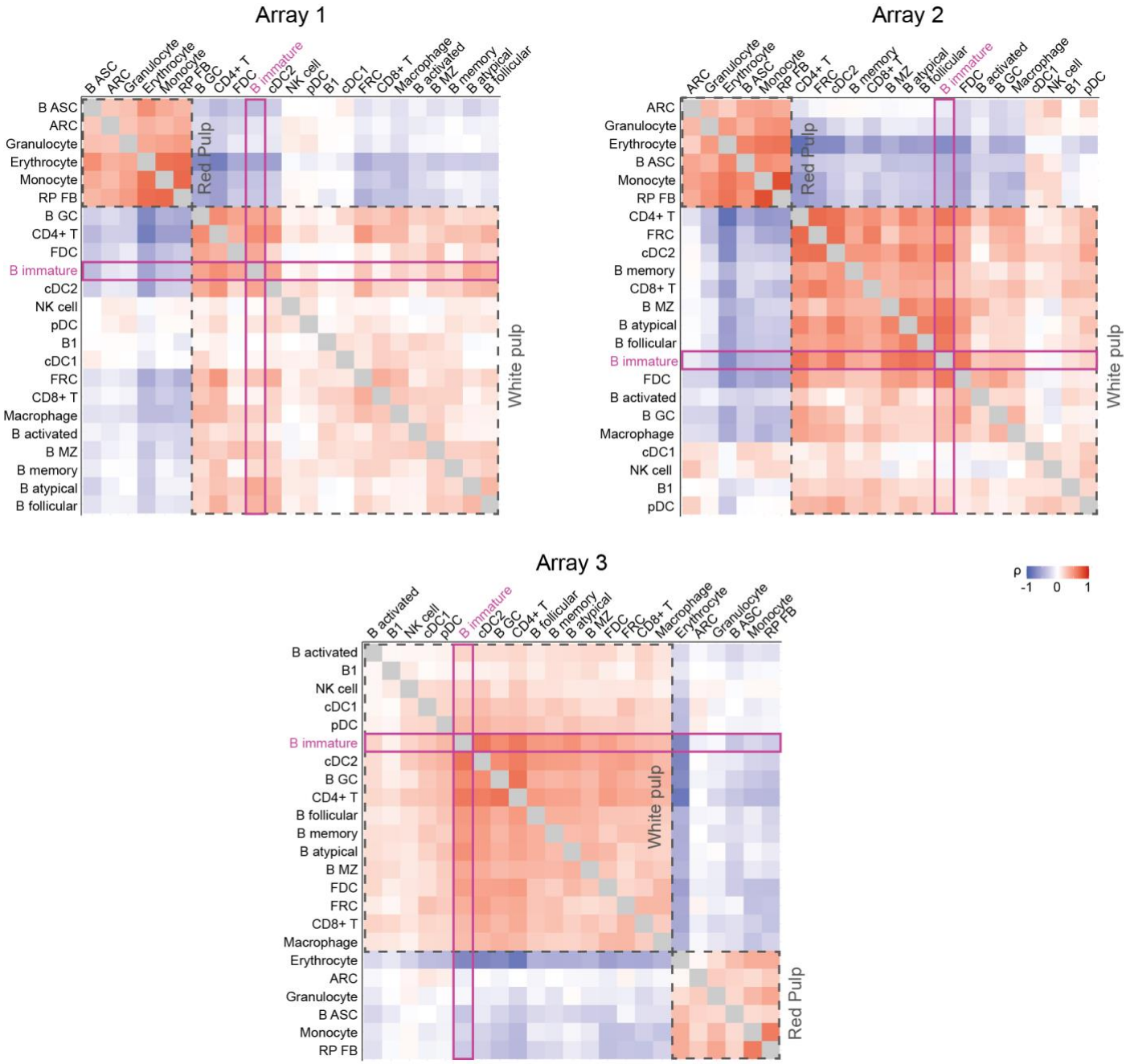

Extended Data Figure 12: Across multiple spatial transcriptomic arrays, immature B cells reside within the white pulp of *Plasmodium* infected spleens.

RCTD spatial deconvolution of immature B cell populations (highlighted in purple) on spatial transcriptomic arrays using *Slide-seqV2* and analysed using spearman's correlation analysis as in Fig. 6D. These arrays are replicates for data shown in Fig. 6D, and combined they comprise two arrays per spleen from two infected mice.

Supplementary Method Figures

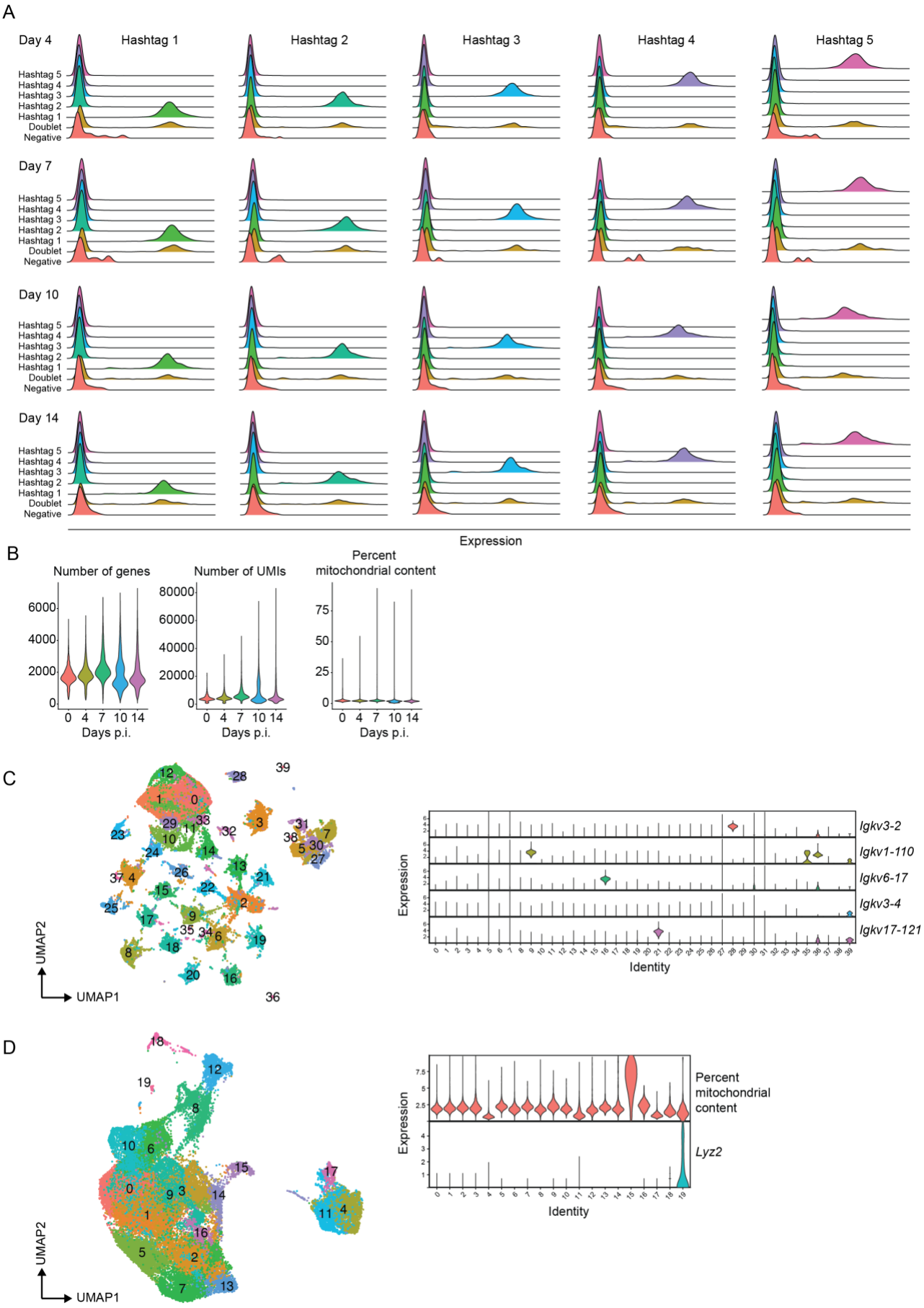

Supplementary Method Figure 1: Quality control for B cell scRNAseq Experiment 1.

(A) Ridge plots for each hashtag showing expression of hashtag oligos for singlets (hashtags 1-5), doublets and negative cells for each timepoint. Note, hashtag 1 in the day 4 group is the day 0, naive B cell sample. (B) Violin plots of number of genes, number of UMIs and percent mitochondrial content prior to pre-processing of data. (C) UMAP of entire B cell dataset after high dimensional reduction and clustering prior to removal of BCR-related genes including violin plots showing distribution of expression of a random selection of BCR related genes for each cluster. (D) UMAP of entire B cell dataset after removal of BCR-related genes and after high dimensional reduction and clustering. Violin plots show the distribution of percent mitochondrial content and *Lyz2* (monocytes) expression per cluster.

A

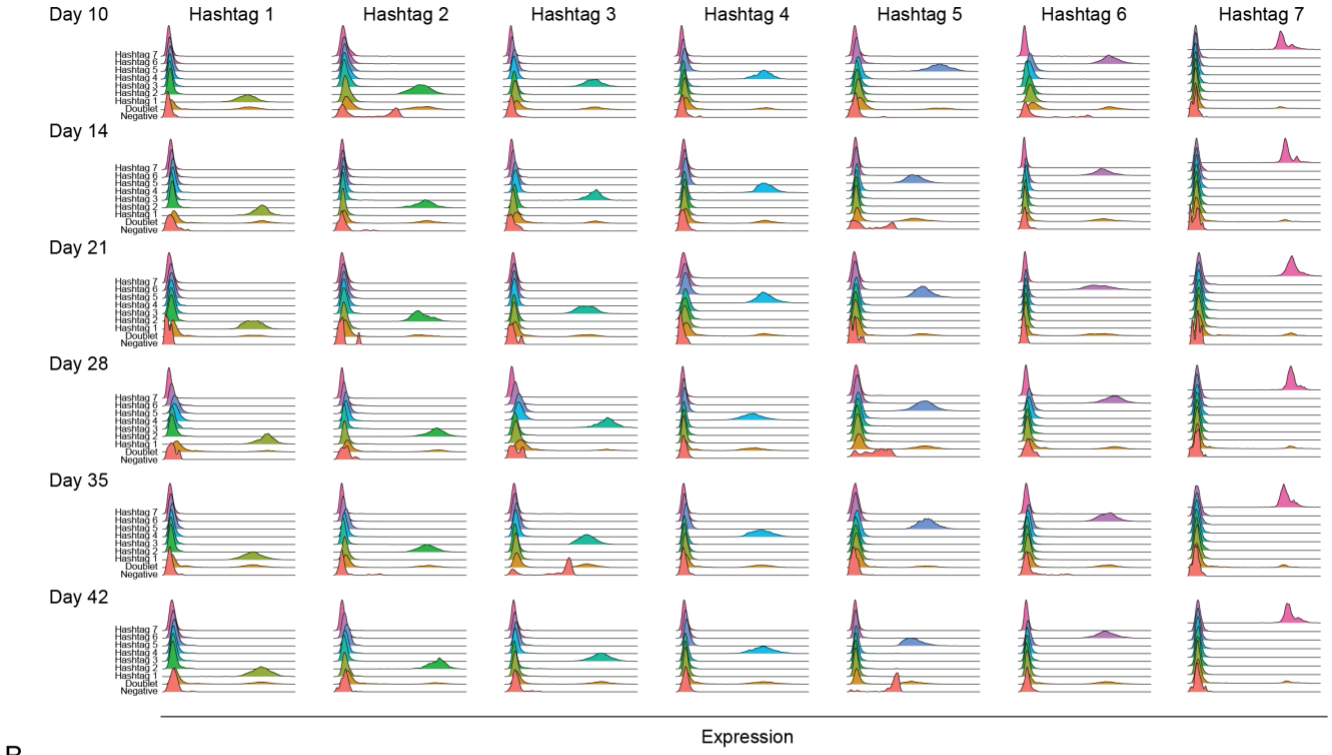
Day 10
Hashtag 1
Hashtag 2
Hashtag 3
Hashtag 4
Hashtag 5
Hashtag 6
Hashtag 7
Day 14
Day 21
Day 28
Day 35
Day 42
Expression

B

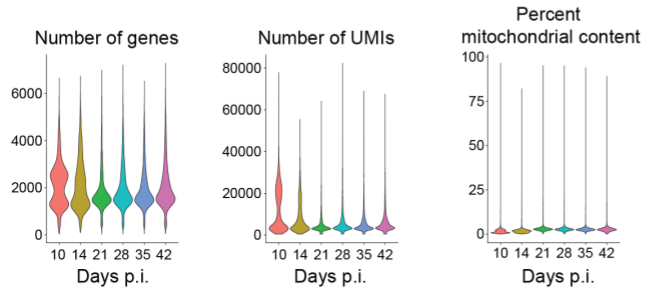
Number of genes
Number of UMIs
Percent mitochondrial content
Days p.i.
10 14 21 28 35 42

C

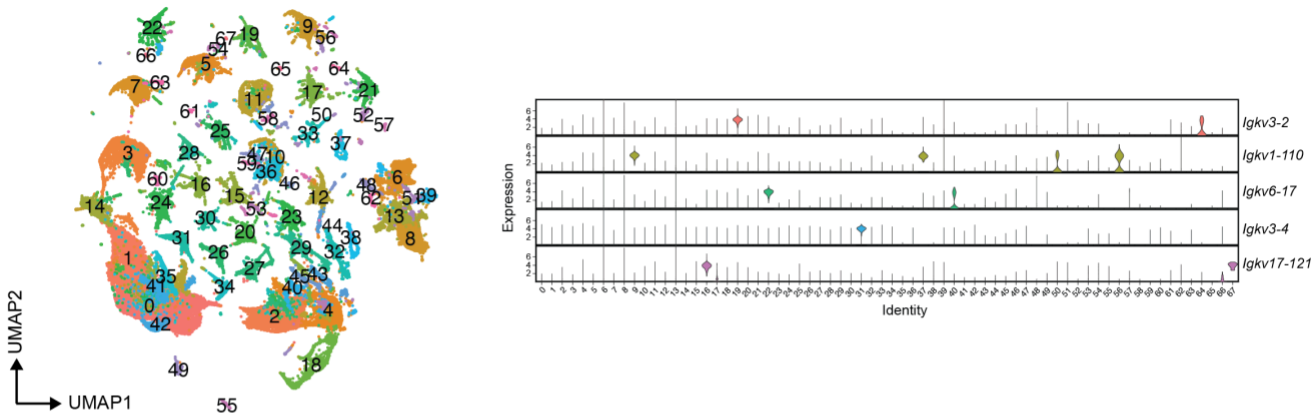
UMAP2
UMAP1
Igkv3-2
Igkv1-110
Igkv6-17
Igkv3-4
Igkv17-121
Expression
Identity

D

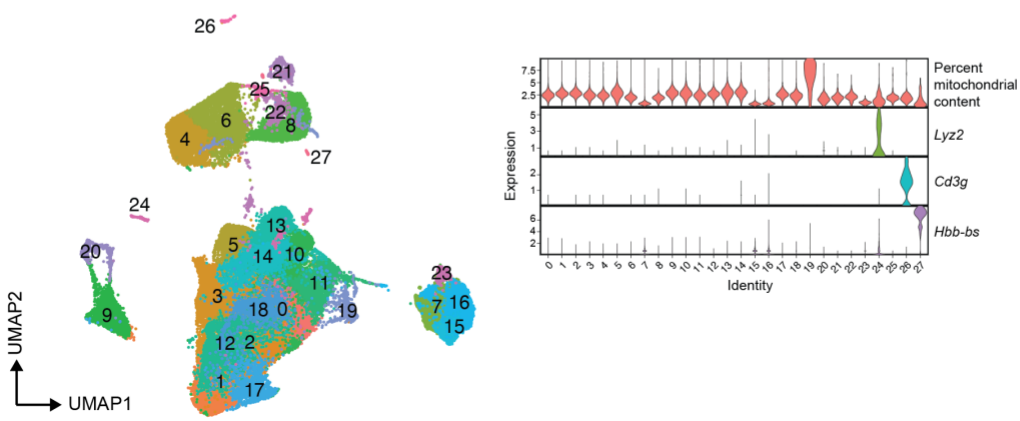
UMAP2
UMAP1
Percent mitochondrial content
Lyz2
Cd3g
Hbb-bs
Expression
Identity

Supplementary Method Figure 2: Quality control for B cell scRNAseq Experiment 2.

(A) Ridge plots for each hashtag showing expression of hashtag oligos for singlets (hashtags 1-7), doublets and negative cells for each timepoint. (B) Violin plots of number of genes, number of UMIs and percent mitochondrial content prior to pre-processing of data. (C) UMAP of entire B cell dataset after high dimensional reduction and clustering prior to removal of BCR-related genes including violin plots showing distribution of expression of a random selection of BCR related genes for each cluster. (D) UMAP of entire B cell dataset after removal of BCR-related genes and after high dimensional reduction and clustering. Violin plots show the distribution of percent mitochondrial content and *Lyz2* (monocytes), *Cd3g* (T cells) and *Hbb-bs* (erythrocytes) expression per cluster.

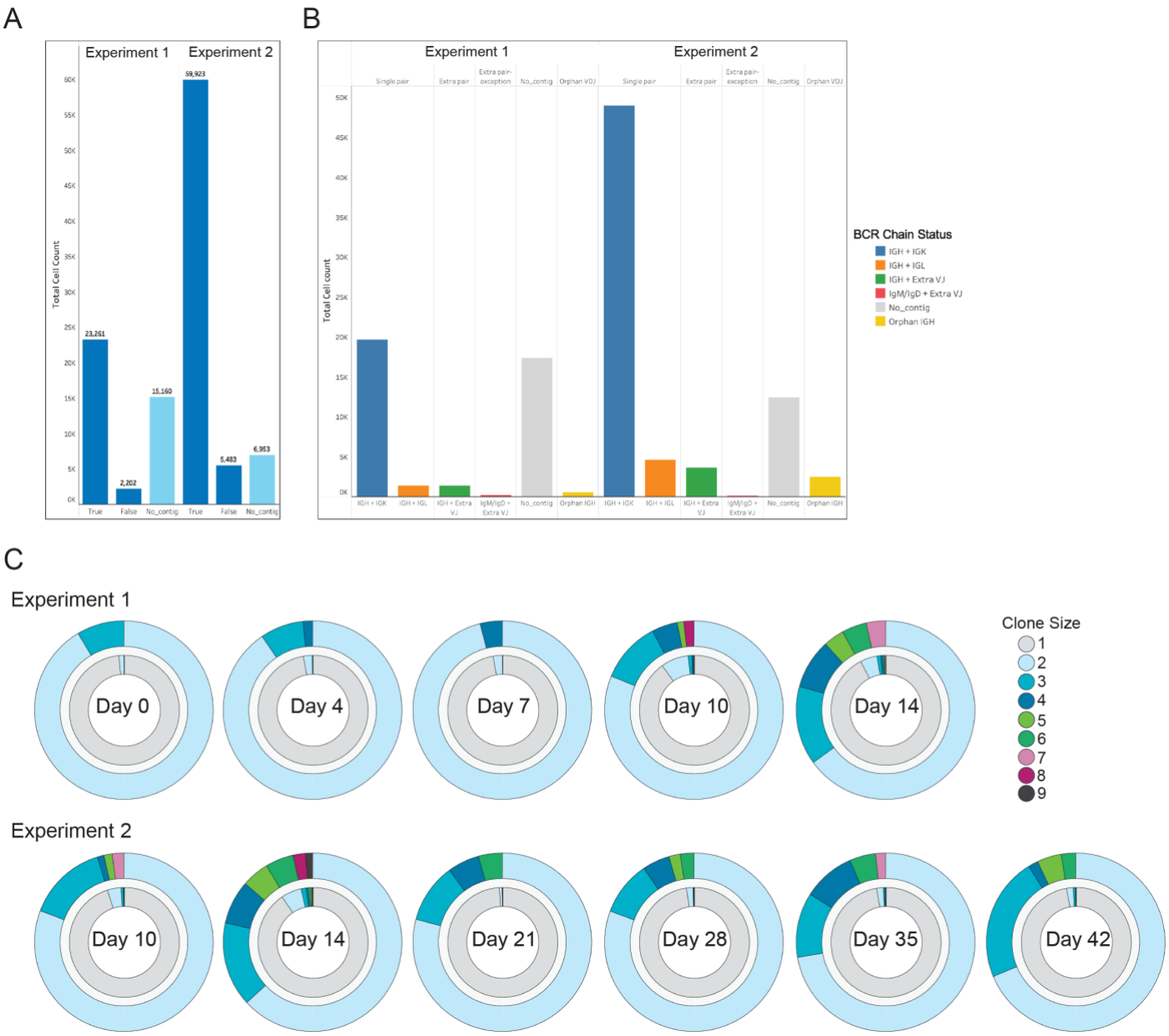

Supplementary Method Figure 3: Quality control of BCR sequencing data.

(A) Bar plot showing distribution of cells which passed Dandelion quality control pipeline for each experiment. (B) Bar plot showing distribution of BCR chains in each experiment. (C) Donut plots showing all clones including unexpanded and expanded clones (inner donut) and expanded clones only (outer donut) at each timepoint for each experiment.

References

1 Stavnezer, J., Guikema, J. E. & Schrader, C. E. Mechanism and regulation of class switch recombination. *Annu Rev Immunol* **26**, 261-292 (2008). https://doi.org/10.1146/annurev.immunol.26.021607.090248

2 Stavnezer, J. & Schrader, C. E. IgH chain class switch recombination: mechanism and regulation. *J Immunol* **193**, 5370-5378 (2014). https://doi.org/10.4049/jimmunol.1401849

3 Mesin, L., Ersching, J. & Victora, G. D. Germinal Center B Cell Dynamics. *Immunity* **45**, 471-482 (2016). https://doi.org/10.1016/j.immuni.2016.09.001

4 Suan, D., Sundling, C. & Brink, R. Plasma cell and memory B cell differentiation from the germinal center. *Curr Opin Immunol* **45**, 97-102 (2017). https://doi.org/10.1016/j.coi.2017.03.006

5 Sutton, H. J. *et al.* Atypical B cells are part of an alternative lineage of B cells that participates in responses to vaccination and infection in humans. *Cell Rep* **34**, 108684 (2021). https://doi.org/10.1016/j.celrep.2020.108684

6 Holla, P. *et al.* Shared transcriptional profiles of atypical B cells suggest common drivers of expansion and function in malaria, HIV, and autoimmunity. *Sci Adv* **7** (2021). https://doi.org/10.1126/sciadv.abg8384

7 Eisen, H. N. & Siskind, G. W. Variations in Affinities of Antibodies during the Immune Response. *Biochemistry* **3**, 996-1008 (1964). https://doi.org/10.1021/bi00895a027

8 Vijay, R. *et al.* Infection-induced plasmablasts are a nutrient sink that impairs humoral immunity to malaria. *Nat Immunol* **21**, 790-801 (2020). https://doi.org/10.1038/s41590-020-0678-5

9 Osier, F. H. *et al.* Breadth and magnitude of antibody responses to multiple Plasmodium falciparum merozoite antigens are associated with protection from clinical malaria. *Infect Immun* **76**, 2240-2248 (2008). https://doi.org/10.1128/IAI.01585-07

10 Rono, J. *et al.* Breadth of anti-merozoite antibody responses is associated with the genetic diversity of asymptomatic Plasmodium falciparum infections and protection against clinical malaria. *Clin Infect Dis* **57**, 1409-1416 (2013). https://doi.org/10.1093/cid/cit556

11 Nkumama, I. N. *et al.* Breadth of Fc-mediated effector function correlates with clinical immunity following human malaria challenge. *Immunity* **57**, 1215-1224 e1216 (2024). https://doi.org/10.1016/j.immuni.2024.05.001

12 Toellner, K. M., Gulbranson-Judge, A., Taylor, D. R., Sze, D. M. & MacLennan, I. C. Immunoglobulin switch transcript production in vivo related to the site and time of antigen-specific B cell activation. *J Exp Med* **183**, 2303-2312 (1996). https://doi.org/10.1084/jem.183.5.2303

13 Pape, K. A. *et al.* Visualization of the genesis and fate of isotype-switched B cells during a primary immune response. *J Exp Med* **197**, 1677-1687 (2003). https://doi.org/10.1084/jem.20012065

14 Roco, J. A. *et al.* Class-Switch Recombination Occurs Infrequently in Germinal Centers. *Immunity* **51**, 337-350 e337 (2019). https://doi.org/10.1016/j.immuni.2019.07.001

15 Taylor, J. J., Pape, K. A., Steach, H. R. & Jenkins, M. K. Humoral immunity. Apoptosis and antigen affinity limit effector cell differentiation of a single naive B cell. *Science* **347**, 784-787 (2015). https://doi.org/10.1126/science.aaa1342

16 Gitlin, A. D. *et al.* Independent Roles of Switching and Hypermutation in the Development and Persistence of B Lymphocyte Memory. *Immunity* **44**, 769-781 (2016). https://doi.org/10.1016/j.immuni.2016.01.011

17 Horton, M. B. *et al.* Lineage tracing reveals B cell antibody class switching is stochastic, cell-autonomous, and tuneable. *Immunity* **55**, 1843-1855 e1846 (2022). https://doi.org/10.1016/j.immuni.2022.08.004

18 de Carvalho, R. V. H. *et al.* Clonal replacement sustains long-lived germinal centers primed by respiratory viruses. *Cell* **186**, 131-146 e113 (2023). https://doi.org/10.1016/j.cell.2022.11.031

19 Hagglof, T. *et al.* Continuous germinal center invasion contributes to the diversity of the immune response. *Cell* **186**, 147-161 e115 (2023). https://doi.org/10.1016/j.cell.2022.11.032

20 King, H. W. *et al.* Single-cell analysis of human B cell maturation predicts how antibody class switching shapes selection dynamics. *Sci Immunol* **6** (2021). https://doi.org/10.1126/sciimmunol.abe6291
21 Espinoza, D. A. *et al.* Distinct stage-specific transcriptional states of B cells derived from human tonsillar tissue. *JCI Insight* **8** (2023). https://doi.org/10.1172/jci.insight.155199
22 Bushell, E. *et al.* Functional Profiling of a Plasmodium Genome Reveals an Abundance of Essential Genes. *Cell* **170**, 260-272 e268 (2017). https://doi.org/10.1016/j.cell.2017.06.030
23 Siddiqui, G. *et al.* A new mass spectral library for high-coverage and reproducible analysis of the Plasmodium falciparum-infected red blood cell proteome. *Gigascience* **11** (2022). https://doi.org/10.1093/gigascience/giac008
24 Venkatesan, P. The 2023 WHO World malaria report. *Lancet Microbe* **5**, e214 (2024). https://doi.org/10.1016/S2666-5247(24)00016-8
25 Sebina, I. *et al.* IFNAR1-Signalling Obstructs ICOS-mediated Humoral Immunity during Non-lethal Blood-Stage Plasmodium Infection. *PLoS Pathog* **12**, e1005999 (2016). https://doi.org/10.1371/journal.ppat.1005999
26 James, K. R. *et al.* IFN Regulatory Factor 3 Balances Th1 and T Follicular Helper Immunity during Nonlethal Blood-Stage Plasmodium Infection. *J Immunol* **200**, 1443-1456 (2018). https://doi.org/10.4049/jimmunol.1700782
27 Habib, T. *et al.* Myc stimulates B lymphocyte differentiation and amplifies calcium signaling. *J Cell Biol* **179**, 717-731 (2007). https://doi.org/10.1083/jcb.200704173
28 Prazma, C. M., Yazawa, N., Fujimoto, Y., Fujimoto, M. & Tedder, T. F. CD83 expression is a sensitive marker of activation required for B cell and CD4+ T cell longevity in vivo. *J Immunol* **179**, 4550-4562 (2007). https://doi.org/10.4049/jimmunol.179.7.4550
29 Zhao, M. *et al.* NF-kappaB subunits direct kinetically distinct transcriptional cascades in antigen receptor-activated B cells. *Nat Immunol* **24**, 1552-1564 (2023). https://doi.org/10.1038/s41590-023-01561-7
30 Lonnberg, T. *et al.* Single-cell RNA-seq and computational analysis using temporal mixture modelling resolves Th1/Tfh fate bifurcation in malaria. *Sci Immunol* **2** (2017). https://doi.org/10.1126/sciimmunol.aal2192
31 Soon, M. S. F. *et al.* Transcriptome dynamics of CD4(+) T cells during malaria maps gradual transit from effector to memory. *Nat Immunol* **21**, 1597-1610 (2020). https://doi.org/10.1038/s41590-020-0800-8
32 Lee, H. J. *et al.* CD4(+) T cells display a spectrum of recall dynamics during re-infection with malaria parasites. *Nat Commun* **15**, 5497 (2024). https://doi.org/10.1038/s41467-024-49879-6
33 Urban, B. C. *et al.* Fatal Plasmodium falciparum malaria causes specific patterns of splenic architectural disorganization. *Infect Immun* **73**, 1986-1994 (2005). https://doi.org/10.1128/IAI.73.4.1986-1994.2005
34 Ssewanyana, I. *et al.* Avidity of anti-malarial antibodies inversely related to transmission intensity at three sites in Uganda. *Malar J* **16**, 67 (2017). https://doi.org/10.1186/s12936-017-1721-3
35 Kennedy, D. E. *et al.* Novel specialized cell state and spatial compartments within the germinal center. *Nat Immunol* **21**, 660-670 (2020). https://doi.org/10.1038/s41590-020-0660-2
36 Mathew, N. R. *et al.* Single-cell BCR and transcriptome analysis after influenza infection reveals spatiotemporal dynamics of antigen-specific B cells. *Cell Rep* **35**, 109286 (2021). https://doi.org/10.1016/j.celrep.2021.109286
37 Tellier, J. *et al.* Unraveling the diversity and functions of tissue-resident plasma cells. *Nat Immunol* **25**, 330-342 (2024). https://doi.org/10.1038/s41590-023-01712-w
38 Lee, R. D. *et al.* Single-cell analysis identifies dynamic gene expression networks that govern B cell development and transformation. *Nat Commun* **12**, 6843 (2021). https://doi.org/10.1038/s41467-021-27232-5
39 Cohen, S., Mc, G. I. & Carrington, S. Gamma-globulin and acquired immunity to human malaria. *Nature* **192**, 733-737 (1961). https://doi.org/10.1038/192733a0

40 Le Bon, A. *et al.* Type i interferons potently enhance humoral immunity and can promote isotype switching by stimulating dendritic cells in vivo. *Immunity* **14**, 461-470 (2001). https://doi.org/10.1016/s1074-7613(01)00126-1
41 Tangye, S. G., Ferguson, A., Avery, D. T., Ma, C. S. & Hodgkin, P. D. Isotype switching by human B cells is division-associated and regulated by cytokines. *J Immunol* **169**, 4298-4306 (2002). https://doi.org/10.4049/jimmunol.169.8.4298
42 Deenick, E. K., Hasbold, J. & Hodgkin, P. D. Decision criteria for resolving isotype switching conflicts by B cells. *Eur J Immunol* **35**, 2949-2955 (2005). https://doi.org/10.1002/eji.200425719
43 Muramatsu, M. *et al.* Specific expression of activation-induced cytidine deaminase (AID), a novel member of the RNA-editing deaminase family in germinal center B cells. *J Biol Chem* **274**, 18470-18476 (1999). https://doi.org/10.1074/jbc.274.26.18470
44 Muramatsu, M. *et al.* Class switch recombination and hypermutation require activation-induced cytidine deaminase (AID), a potential RNA editing enzyme. *Cell* **102**, 553-563 (2000). https://doi.org/10.1016/s0092-8674(00)00078-7
45 Sundling, C. *et al.* Positive selection of IgG(+) over IgM(+) B cells in the germinal center reaction. *Immunity* **54**, 988-1001 e1005 (2021). https://doi.org/10.1016/j.immuni.2021.03.013
46 Jacob, J., Przylepa, J., Miller, C. & Kelsoe, G. In situ studies of the primary immune response to (4-hydroxy-3-nitrophenyl)acetyl. III. The kinetics of V region mutation and selection in germinal center B cells. *J Exp Med* **178**, 1293-1307 (1993). https://doi.org/10.1084/jem.178.4.1293
47 Belyaev, N. N. *et al.* Induction of an IL7-R(+)c-Kit(hi) myelolymphoid progenitor critically dependent on IFN-gamma signaling during acute malaria. *Nat Immunol* **11**, 477-485 (2010). https://doi.org/10.1038/ni.1869
48 Haltalli, M. L. R. *et al.* Manipulating niche composition limits damage to haematopoietic stem cells during Plasmodium infection. *Nat Cell Biol* **22**, 1399-1410 (2020). https://doi.org/10.1038/s41556-020-00601-w
49 Ghosn, E. E., Sadate-Ngatchou, P., Yang, Y., Herzenberg, L. A. & Herzenberg, L. A. Distinct progenitors for B-1 and B-2 cells are present in adult mouse spleen. *Proc Natl Acad Sci U S A* **108**, 2879-2884 (2011). https://doi.org/10.1073/pnas.1019764108
50 Ghosh, D. *et al.* An Atypical Splenic B Cell Progenitor Population Supports Antibody Production during Plasmodium Infection in Mice. *J Immunol* **197**, 1788-1800 (2016). https://doi.org/10.4049/jimmunol.1502199
51 Lee, M. S. J. *et al.* Acute malaria suppresses the B lymphocytic niche in the bone marrow through the alteration of CXCL12-abundant reticular cells. *Int Immunol* **36**, 339-352 (2024). https://doi.org/10.1093/intimm/dxae012
52 Kallies, A. *et al.* Plasma cell ontogeny defined by quantitative changes in blimp-1 expression. *J Exp Med* **200**, 967-977 (2004). https://doi.org/10.1084/jem.20040973
53 Pracht, K. *et al.* A new staining protocol for detection of murine antibody-secreting plasma cell subsets by flow cytometry. *Eur J Immunol* **47**, 1389-1392 (2017). https://doi.org/10.1002/eji.201747019
54 Akter, J. *et al.* Plasmodium-specific antibodies block in vivo parasite growth without clearing infected red blood cells. *PLoS Pathog* **15**, e1007599 (2019). https://doi.org/10.1371/journal.ppat.1007599
55 Hao, Y. *et al.* Integrated analysis of multimodal single-cell data. *Cell* **184**, 3573-3587 e3529 (2021). https://doi.org/10.1016/j.cell.2021.04.048
56 Sundell, T. *et al.* Single-cell RNA sequencing analyses: interference by the genes that encode the B-cell and T-cell receptors. *Brief Funct Genomics* **22**, 263-273 (2022). https://doi.org/10.1093/bfgp/elac044
57 Chen, J., Bardes, E. E., Aronow, B. J. & Jegga, A. G. ToppGene Suite for gene list enrichment analysis and candidate gene prioritization. *Nucleic Acids Res* **37**, W305-311 (2009). https://doi.org/10.1093/nar/gkp427

58 Liao, Y., Wang, J., Jaehnig, E. J., Shi, Z. & Zhang, B. WebGestalt 2019: gene set analysis toolkit with revamped UIs and APIs. *Nucleic Acids Res* **47**, W199-W205 (2019). https://doi.org/10.1093/nar/gkz401

59 Santos, A., Wernersson, R. & Jensen, L. J. Cyclebase 3.0: a multi-organism database on cell-cycle regulation and phenotypes. *Nucleic Acids Res* **43**, D1140-1144 (2015). https://doi.org/10.1093/nar/gku1092

60 Mabbott, N. A. & Gray, D. Identification of co-expressed gene signatures in mouse B1, marginal zone and B2 B-cell populations. *Immunology* **141**, 79-95 (2014). https://doi.org/10.1111/imm.12171

61 Lopez, R., Regier, J., Cole, M. B., Jordan, M. I. & Yosef, N. Deep generative modeling for single-cell transcriptomics. *Nat Methods* **15**, 1053-1058 (2018). https://doi.org/10.1038/s41592-018-0229-2

62 Wolf, F. A., Angerer, P. & Theis, F. J. SCANPY: large-scale single-cell gene expression data analysis. *Genome Biol* **19**, 15 (2018). https://doi.org/10.1186/s13059-017-1382-0

63 Stickels, R. R. *et al.* Highly sensitive spatial transcriptomics at near-cellular resolution with Slide-seqV2. *Nat Biotechnol* **39**, 313-319 (2021). https://doi.org/10.1038/s41587-020-0739-1

64 Williams, C. G. *et al.* Plasmodium infection induces phenotypic, clonal, and spatial diversity among differentiating CD4(+) T cells. *Cell Rep* **43**, 114317 (2024). https://doi.org/10.1016/j.celrep.2024.114317

65 Cable, D. M. *et al.* Robust decomposition of cell type mixtures in spatial transcriptomics. *Nat Biotechnol* **40**, 517-526 (2022). https://doi.org/10.1038/s41587-021-00830-w

66 Alexandre, Y. O. *et al.* A diverse fibroblastic stromal cell landscape in the spleen directs tissue homeostasis and immunity. *Sci Immunol* **7**, eabj0641 (2022). https://doi.org/10.1126/sciimmunol.abj0641

67 Suo, C. *et al.* Dandelion uses the single-cell adaptive immune receptor repertoire to explore lymphocyte developmental origins. *Nat Biotechnol* (2023). https://doi.org/10.1038/s41587-023-01734-7